2018

Analysis of Orbital Friction Welding for Titanium Blades on Compressor Drum

Karan Shirish Antrolia
Lehigh University, antrolia.karan@gmail.com

Analysis of Orbital Friction Welding for Titanium Blades on Compressor Drum

by

Karan S. Antrolia

A Thesis

Presented to the Graduate and Research Committee

of Lehigh University

in Candidacy for the Degree of

Master of Science

In

Mechanical Engineering

Lehigh University

May 2018

This thesis is accepted and approved in partial fulfillment of the requirements for the Master of Science.

_____

Date

_____

Thesis Advisor

_____

Chairperson of Department

Acknowledgments

I would like to thank Professor Herman Nied, foremost for an opportunity to work on this and other research projects. With his unyielding support, patience, and encouragement he helped me discover, understand and solve problems I previously would not have discovered. Prof. Nied shaped my thought process regarding research and taught me how to approach a problem. I am sincerely grateful for this experience as a student, research fellow and a professional.

I would also like to thank my parents and my brother for all the love, care, and support. My fellow graduate students are also thanked for all the help, guidance and love.

Table of Contents

List of Figures

Abstract

The Orbital friction welding process utilizes high heat generated at the interface from friction to form a high strength weld. A full transient thermal 3D analysis combined with axial displacement was conducted using ANSYS to simulate this welding process. The goal was to model the process of orbital friction welding by incorporating industry-relevant parameters under realistic boundary conditions. The work illustrates the dependency of the temperature profile on various processing parameters at any point in time in the welding process. The mathematical results are compared and analyzed with measured experimental data. The numerical model is used to predict the temperature flow in orbital friction welding under typical process conditions.

Chapter 1

Introduction to Friction Welding

Under normal manufacturing conditions, thermal energy generated due to friction is considered to be an undesirable by-product but in the process of friction welding, thermal energy generated from friction is used to produce a high-quality weld. Friction welding is a solid-state process wherein one coupon is set in motion relative to another coupon while under pressure contact resulting in frictional heat generation on the interface, the mating surface; see Figure 1 (a). Due to the heat generated by the mechanical friction and the compressive force applied once the motion ceases, the interface is plasticized creating the diffusion bond [1]–[3]. Impurities such as oxides and alien particles which may affect the weld quality adversely are expelled through flash [4]; see Figure 1 (b).

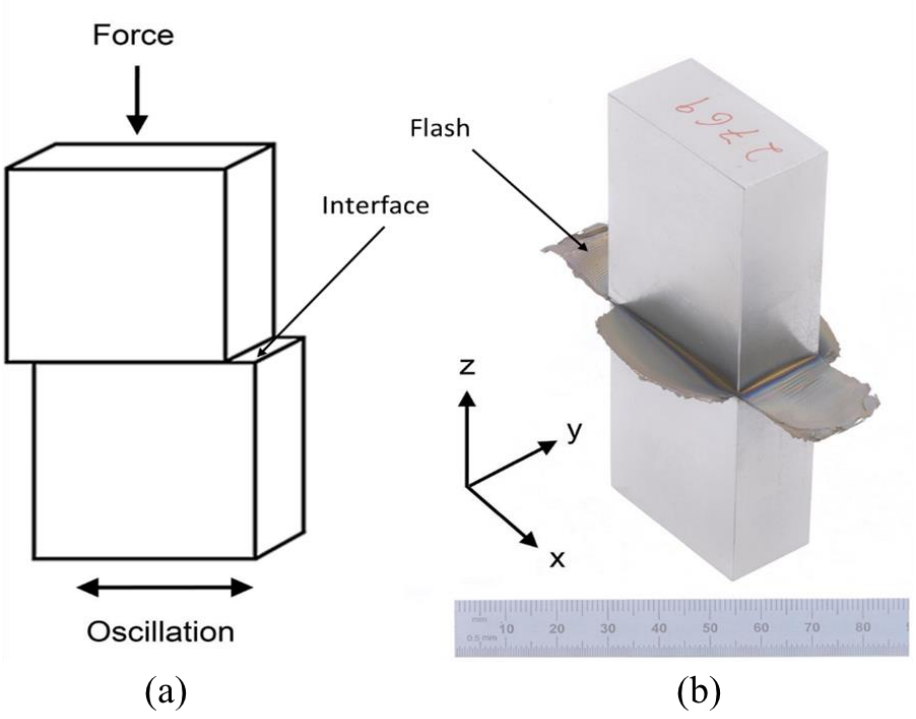

Figure 1. (a) Linear friction welding process schematic

and (b) Flash expelled [3]

Linear, Rotary, and Orbital are the three fundamental types of friction welding [1]. Figure 1 (a) depicts linear friction welding (LFW) wherein one coupon oscillates in a reciprocal motion, while under pressure contact with respect to the other coupon. In the case of rotary friction welding, one coupon is rotated against another coupon which is usually held stationary, while under frictional pressure; see Figure 2. Rotary friction welding is limited to axisymmetric components [1]. Linear friction welding and orbital friction welding are an extension of the friction welding process to non-axisymmetric components. Orbital Friction Welding (OFW) is a solid-state process in which both the coupons are orbited with respect to each other around their common longitudinal axes, while pressed against each other with their longitudinal axes parallel and offset; see Figure 3. As the motion ceases the axes needs to be realigned before the forging force is applied [1][2].

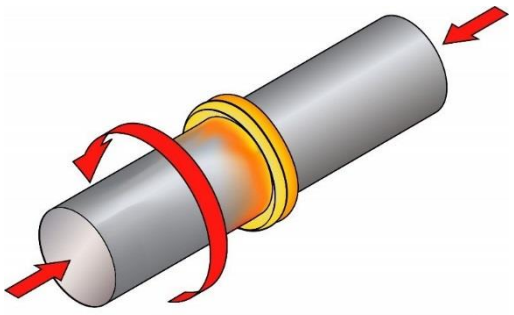

Figure 2. Rotary friction process schematic [5]

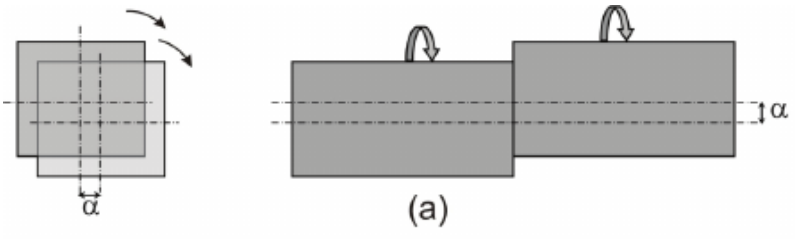

Figure 3. Orbital friction welding process schematic [2]

The friction welding process can be described in four stages [1], [4], [6].

Phase I: Contact surface area increases due to asperity wear resulting in heat generation through friction.

Phase II: Interface material changes and becomes highly deformable under relatively low pressure but no change of state occurs.

Phase III: Flash expulsion initiates, heat is generated due to plastic deformation.

Phase IV: Relative motion ceases and both the coupons are realigned. Once realigned forging force is applied resulting in the formation of a diffusion bond due to the expulsion of highly plasticized material.

Comparison between linear and orbital friction welding can be drawn as all the four phases are observed in both processes. The difference between LFW and OFW lies in the volume of heat generated in the first two phases. The volume of frictional heat generated in OFW process is higher than LFW process resulting in the shorter time period required for OFW process as compared to LFW process [6]. More material is extruded in OFW process than LFW process even though process time is shorter. Due to the nature of relative motion in-between coupons, additional distance is covered in a single period in OFW process than LFW process resulting in higher surface power density values [6]. To summarize OFW process is more efficient than LFW process.

Chapter 2

Mathematical Model

2.1 Welding Process

A specific orbital friction welding process of interest involves the welding of blades to a compressor drum. This is a critical aircraft engine component that requires very high-quality welds. The component in relative orbital motion is the blade with the static component of the drum; see Figure 4.

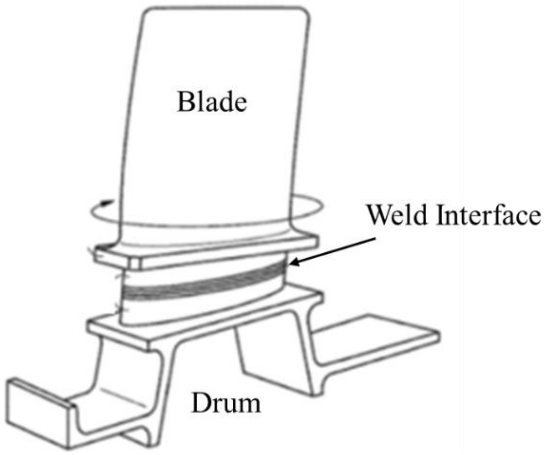

Figure 4. Blade to drum weld geometry

Weld interface material is Ti-6Al-4V/ Ti-6Al-4V; see Figure 4. Titanium alloys are chosen because of material properties such as high strength to weight ratio, corrosion resistance and mechanical properties at elevated temperatures.

The frequency of orbital motion is kept constant throughout the welding process. This particular OFW process is divided into the following three steps:

- Step I: Frictional rotation is initiated making the interface material highly deformable without any change of state.

- Step II: Frictional motion resulting in material softening all along the interface.
- Step III: Blades are realigned as frictional motion ceases and calculated forging force is applied.

2.2 Process Parameters

For analysis of the OFW process, the welding parameters and the material properties are required. A range of parameters is controlled and monitored throughout the OFW process. The following list of parameters are controlled during the OFW process:

- Orbital Frequency
- Orbital Amplitude
- Forging Force Applied
- Forging Time
- Material Consumed in Steps I & II

The following list of parameters can be monitored during the OFW process:

- Time
- Orbital Frequency
- Piston Pressure
- Displacement of Blade
- Machine Power Delivered
- Motion orbital Torque

Machine Power Delivered is the gross amount of electrical energy consumed for the Orbital Friction welding of a single blade to a compressor drum.

2.3 Finite Element Modelling Strategy

The objective is to develop an analytical model to predict thermal characterization of the orbital frictional welding process used in welding of a blade to the drum; see Figure 5.

Figure 5. Bladed Drum

There are two approaches to develop an analytical model regarding OFW process. One approach is to model the detailed physics of frictional surfaces in contact. This approach is quite difficult because it requires the modeling to take into consideration the mechanics, chemistry and atomistic interactions of the two surfaces in frictional contact. The second approach employs a semi-empirical model which incorporates the material behavior while utilizing empirical models to characterize the heat flux generated due to friction at the interface.

The simulation presented here is based on the second approach applied in the software package ANSYS [7].

2.4 Material Properties

ANSYS material library does not contain the required weld interface materials. To generate temperature distribution fields and temperature profiles for specific positions thermal properties of the titanium alloy Ti-6Al-4V are required. Required thermal material properties are imported into ANSYS from [8]; see Figure 6 – 8.

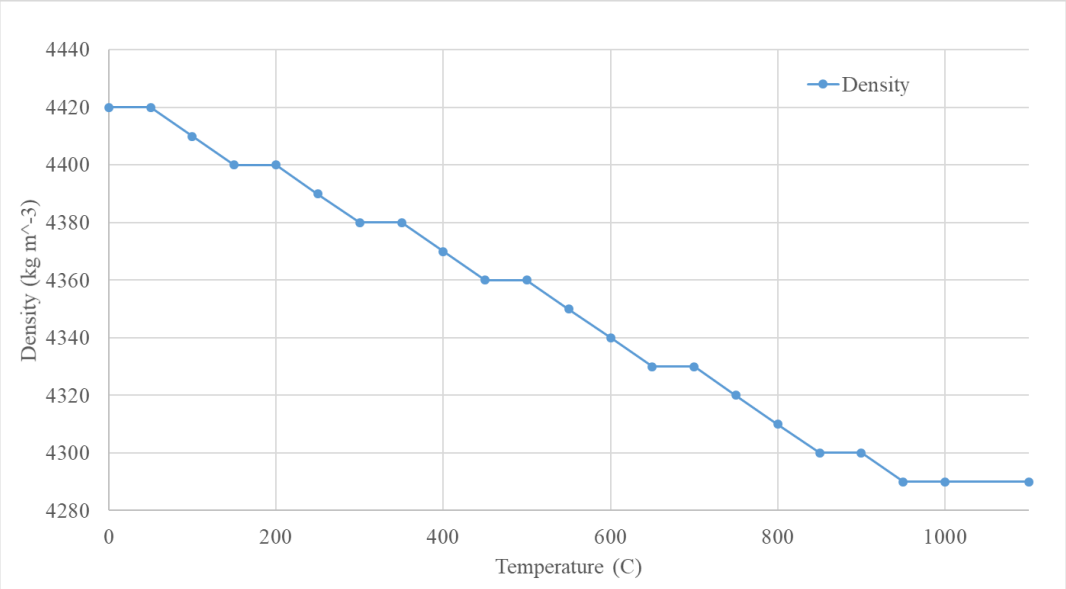

Figure 6. Density vs Temperature Ti-6Al-4V [8]

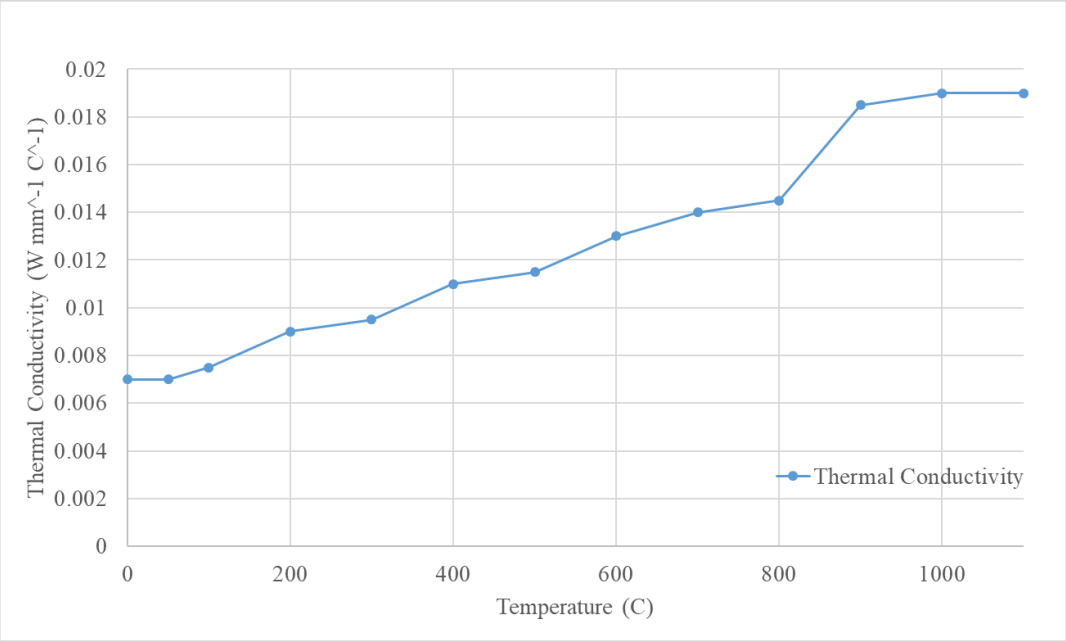

Figure 7. Thermal Conductivity vs Temperature Ti-6Al-4V [8]

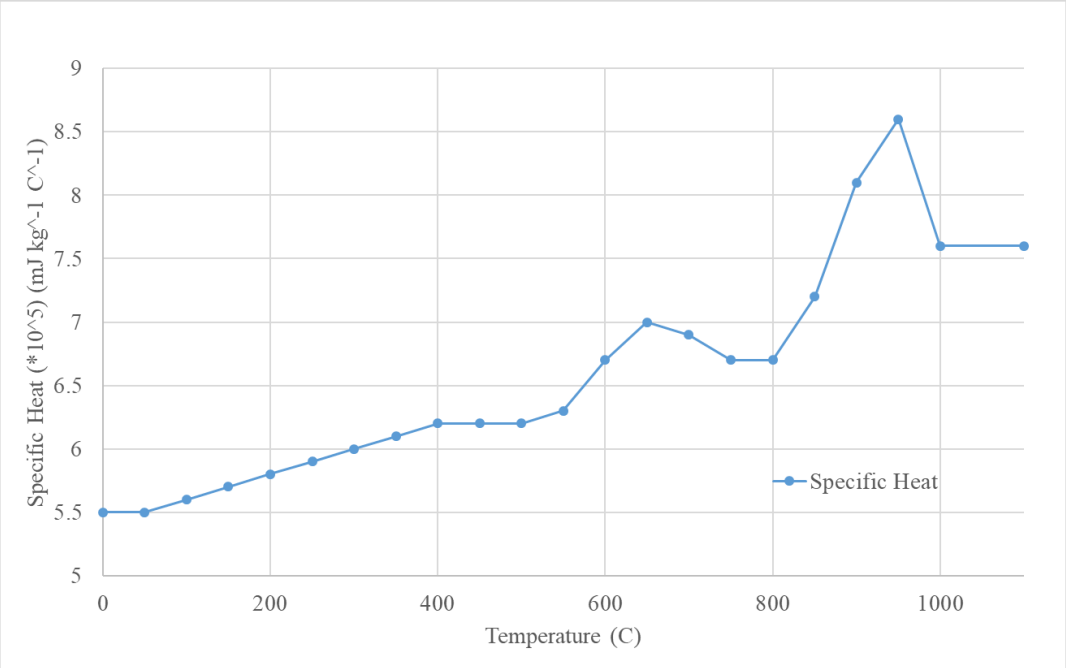

Figure 8. Specific Heat vs Temperature Ti-6Al-4V [8]

2.5 Geometry

Coupons with three different interface surface areas were selected for OFW process analysis; see Figure 9. For OFW process parameter measurements, two coupons with identical surface areas were welded. In some loose sense, one surface represents the blade and the other represents the platform on the drum. Heat generation at the weld interface due to friction dictates the overall thermomechanical behavior during the OFW process. Thus, the interface surface area is a critical parameter for the simulation. The selected coupon geometries used in this study are based on simplified versions of the final blade surface contact zones. A simplified version of the coupon is chosen to circumvent the higher cost of welding experiments on the complex blade-shaped coupons.

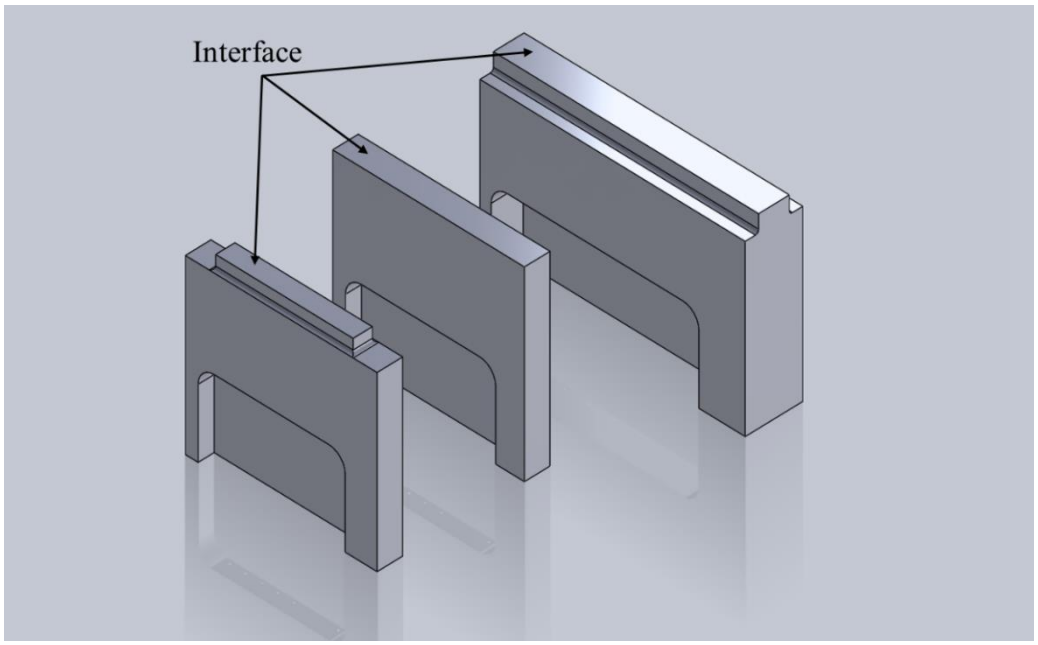

Figure 9. Three coupons with increasing interface surface area

A total of five thermocouples are placed inside each coupon; see Figure 10. Thermal data measured during the welding process by thermocouples was utilized to calibrate the efficiency factor for simulations. The efficiency factor is the fraction of the gross electrical power delivered to the machine that was utilized for the creation of frictional heat at the interface.

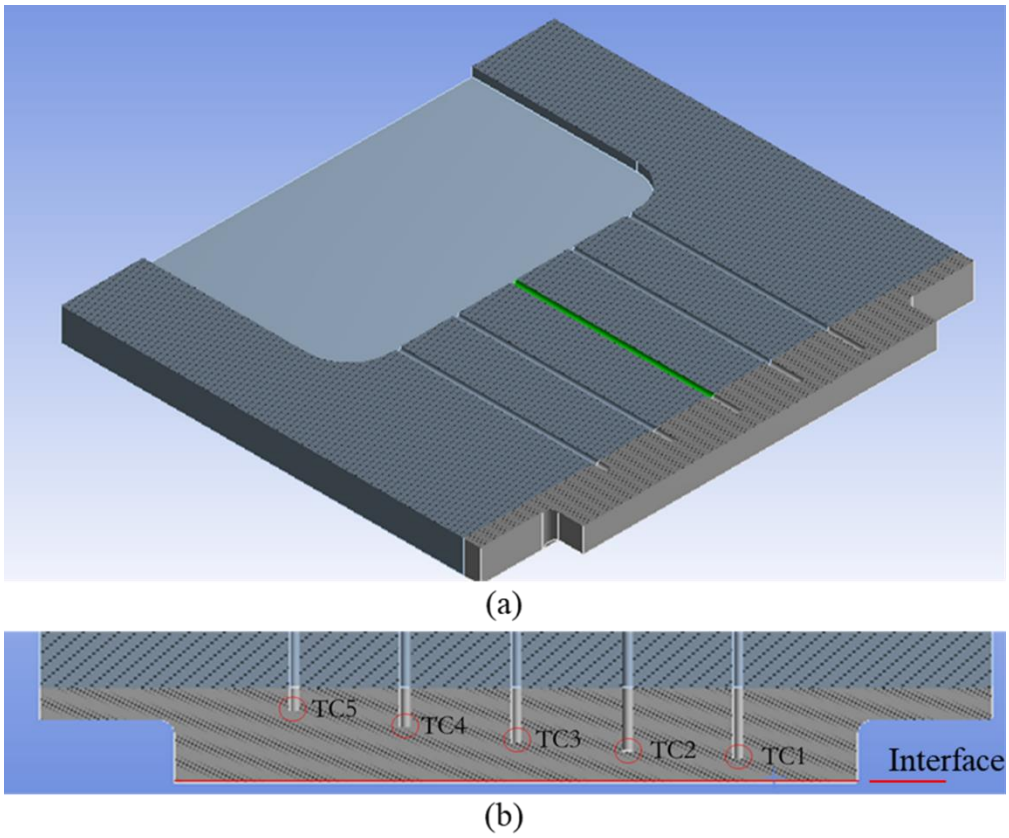

Figure 10. (a) Coupon cross-section exhibiting Thermocouple holes and

(b) Magnified view to exhibit distance between Thermocouples and the interface

2.6 Meshing

Mesh density was chosen along the interface up to a certain depth based on the steepest temperature gradients observed [2], [9]. Fine elements were applied from the interface up to a certain depth depending upon the thermocouple placement of the model under consideration; see Figure 11 (a). As the material properties are strongly temperature dependent and the OFW process duration is hardly a few seconds mesh density is critical. The heat-affected zone is of short length from the weld interface. Therefore only a small section of the finite element model near the welding interface is finely meshed and utilized for OFW process analysis [9]. In thermal finite element simulations using ANSYS, SOLID87 a 3-D, 10-Node Tetrahedral [10]; see Figure 11 (b) and SOLID90 a 3-D, 20-Noded with quadratic shape function elements are employed [10]; see Figure 11 (c).

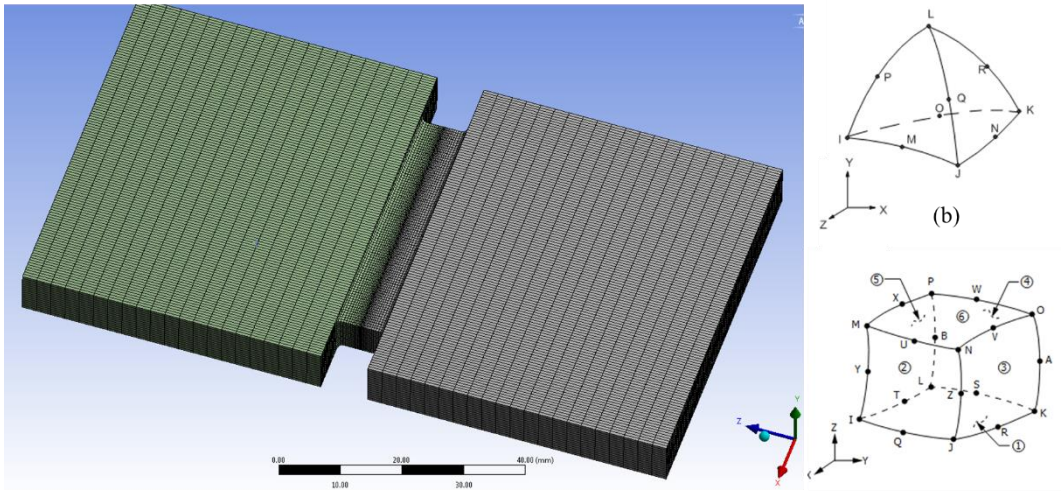

Figure 11. (a) Model representing mesh density, (b) SOLID87 and (c) SOLID90

2.7 Frictional Heat Flux – Load definition

Heat flux generated at the interface is the key to the thermo-mechanical behavior of the coupon. Here, frictional heat flux at the interface is characterized by utilizing empirical models. One of the monitored process parameters is machine power delivered throughout the OFW process; see Figure 12. The experimentally measured power data against time is adequate to define the heat flux generated by frictional contact at the interface [11]. As all the power applied to the OFW process is not going to be converted to frictional heat, an efficiency factor needs to be derived by calibrating the computational results with temperatures recorded by the thermocouples.

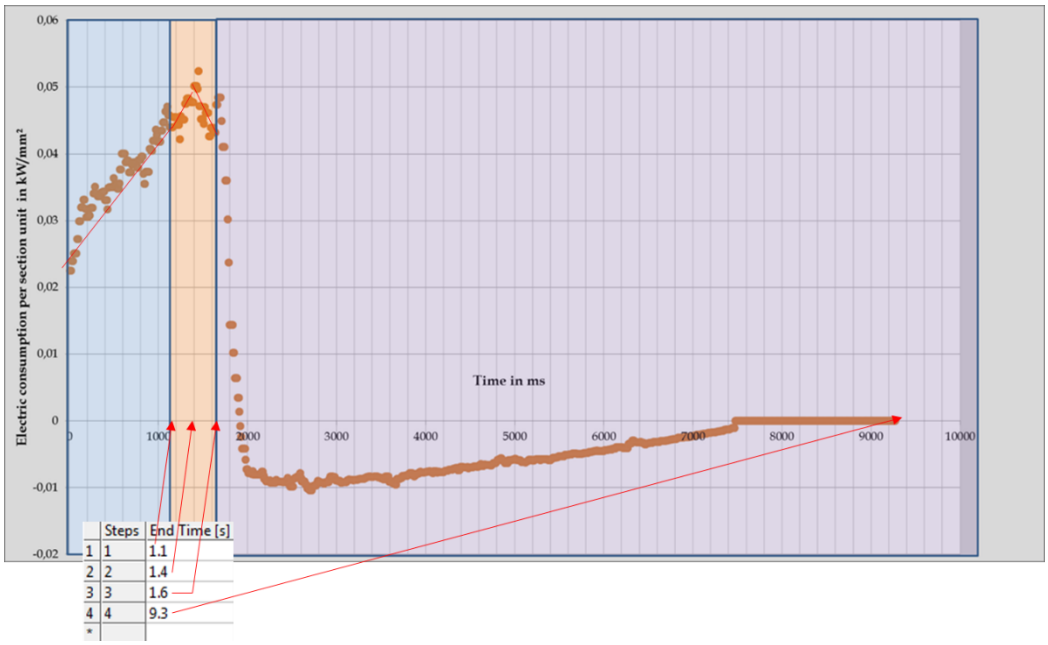

Figure 12. Electrical Power Consumption recorded, divided as per three stages

The heat flux derived from power consumption measured throughout the OFW process was divided as per three stages of the OFW process; see Figure 12. Four positions in time were selected as load steps of heat flux input to ANSYS; see Figure 12. Heat generated through friction was refined and calibrated to be applied on the interface in the transient thermal analysis of the OFW process in ANSYS; see Figure 13. Heat flux input values shown in Figure 13 are from a test case, determined to be at an efficiency of 30% for one set of coupons to test the convergence of the model.

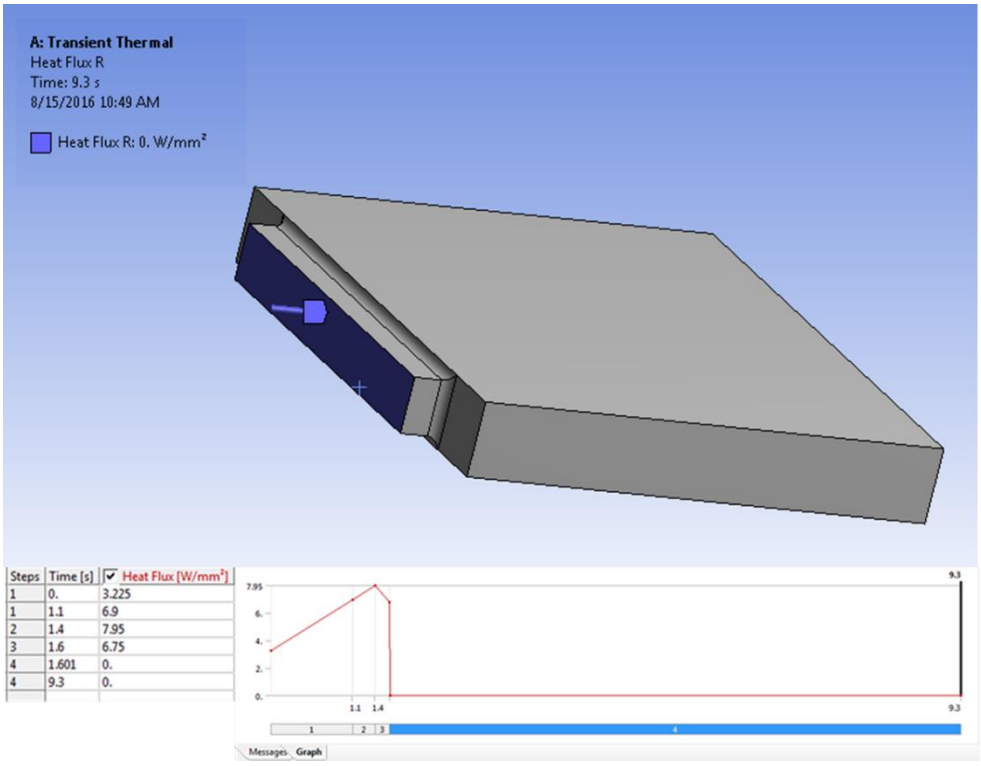

Figure 13. Heat Flux derived from Electric power consumption applied uniformly across the interface of a transient thermal model

2.8 Boundary Conditions

Various works have been published addressing numerical modeling of friction welding. One of the foremost and common assumptions across various analytical models predicting thermal and mechanical behavior for linear and orbital friction welding is of uniform heat generation and pressure across the interface; see Figure 13 [2], [11]–[13]. This assumption is also proved mathematically for small values of amplitude [14].

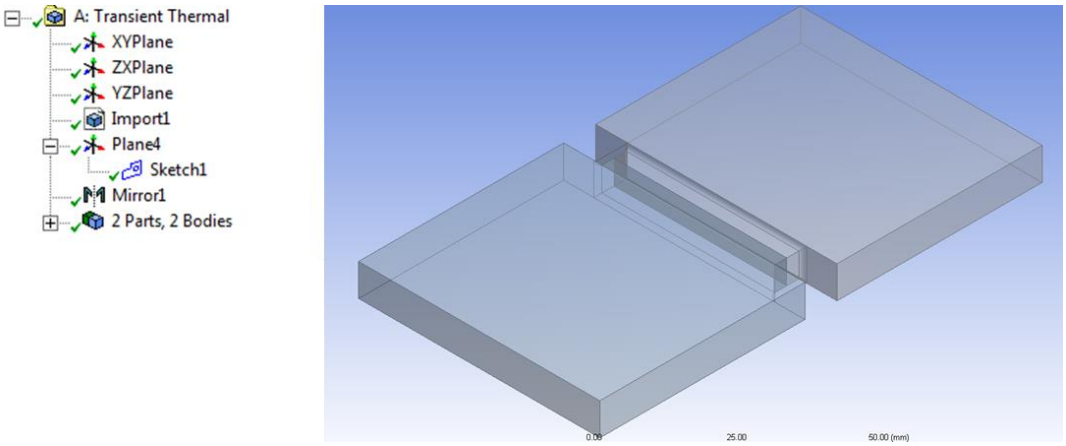

Figure 14. Analytical model exhibiting the symmetrical nature

Due to the symmetrical nature of the problem; see Figure 14, only a single coupon is modeled [2], [9], [12], [13], while symmetry conditions are applied at the interface; see Figure 13. Also reducing the number of elements helps in executing the simulation in a fraction of the time taken otherwise. Depending on the geometry of the model only a quarter section of a single coupon needs to be modeled.

For OFW, the coupon in relative motion is held by a fixture throughout the duration of the process. For OFW the frictional heat generated will dissipate through conduction, convection, and radiation. The bulk of the coupon is enclosed in a fixture throughout the welding cycle which results in heat loss primarily through conduction; see Figure 15. A portion of the coupons near the interface is open to the atmosphere resulting in some heat loss through convection and radiation; see Figure 16. When all three heat loss boundary conditions have been applied, the difference in the approximation of the measured temperature profile was ± 0.5% as compared to not applying any heat loss boundary conditions.

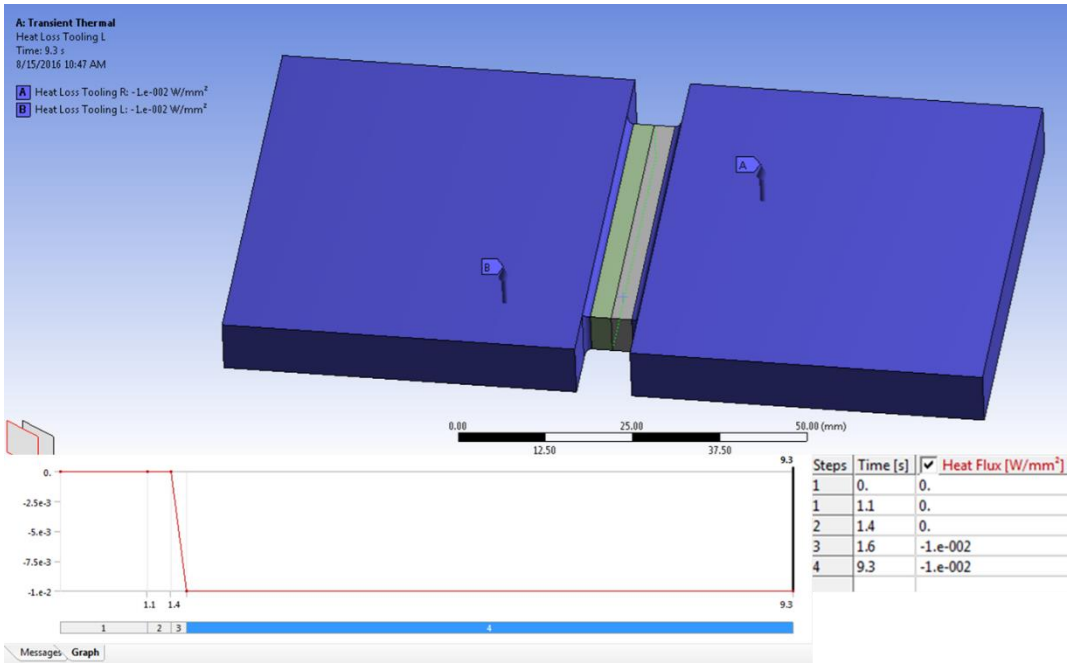

Figure 15. Heat loss through Conduction

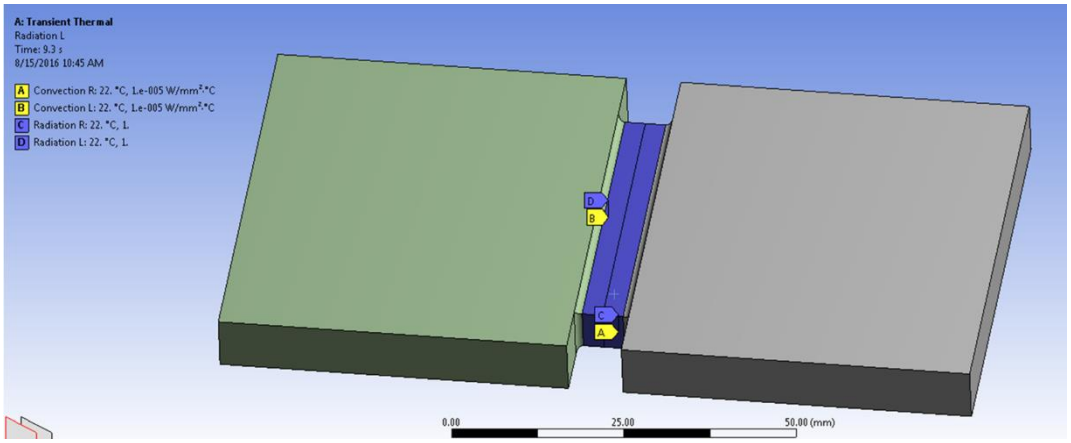

Figure 16. Exhibiting Convection and Radiation boundary conditions

on analytical model

For a majority of the simulations carried out for calibration of the numerical model to recorded temperatures, heat loss boundary conditions can be omitted as the process happens so rapidly that insignificant amount of heat has time to escape from the coupon surfaces during the critical measurement period. Of course, much later in time, the welded part cools down due to conduction into the fixture and convective cooling to the air. Apply heat loss boundary conditions during the final phase of calibration to fine-tune the simulation approximations. Omitting the heat loss boundary conditions for the initial phase of simulations has the benefit of reducing the computational time by 35%.

The OFW process has a short duration of ~9.3 seconds in which heat loss is limited to a small extent. Limited heat loss might be due to the short duration of the weld cycle or considerably higher heat generated dwarfing the heat loss.

Considering that the effect of heat loss from the boundaries of the coupon is negligible, the base of the coupon which is held by the fixture and responsible for heat loss due to conduction can be cut down; see Figure 17. The cut model increases the simulation efficiency by reduction of elements without a significant effect on thermal approximations. Implementation is recommended in the initial phase of simulations.

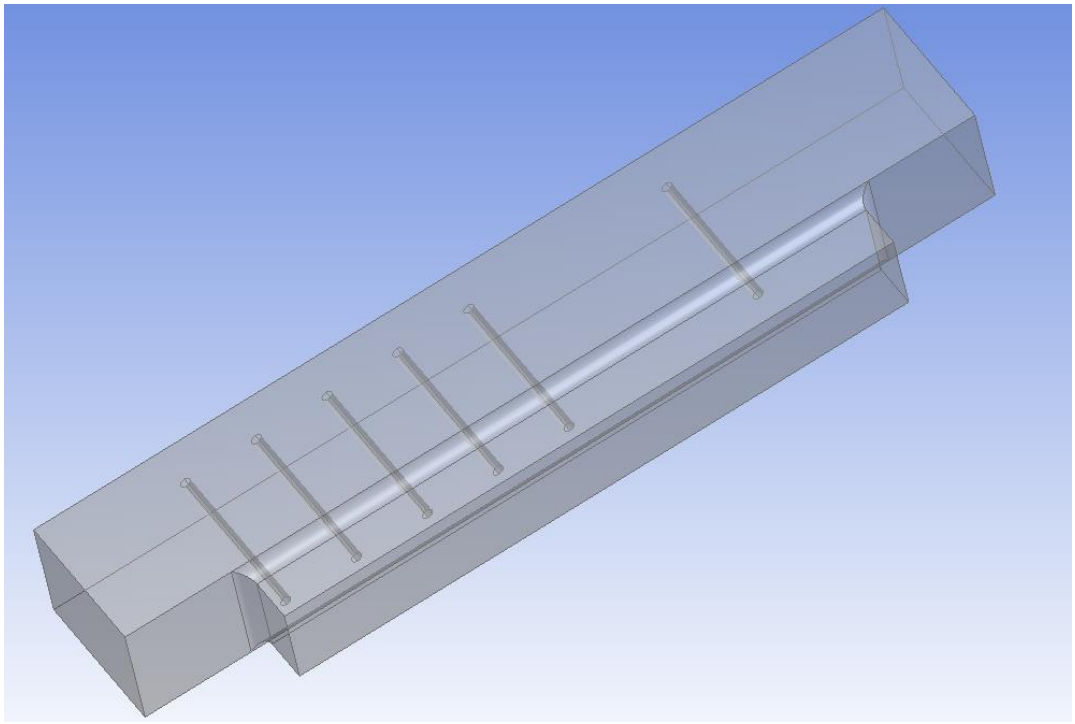

Figure 17. Cut model

Chapter 3

Results and Model Modification

3.1 Results and discussion – the first round of coupons

Two sets of similar coupons are welded under the exact same conditions in the first round of experiments. The temperature profile from each set is determined and employed for calibration of efficiency factor. Calibration of efficiency factor here is achieved by curve fitting of temperature profile produced through simulations to the experimentally measured temperature profiles. For thermal simulations of the first round of coupons, the aforementioned boundary conditions are applied. The heat flux applied at the interface in mathematical models is derived from the electrical power consumption measured during the welding process.

Following are temperature profile comparisons in between the temperature profile prediction from simulations and average of the experimentally measured temperature profile of each set; Figure 19 - Figure 23. For reference thermocouple map used during welding of both the sets is provided; see Figure 18.

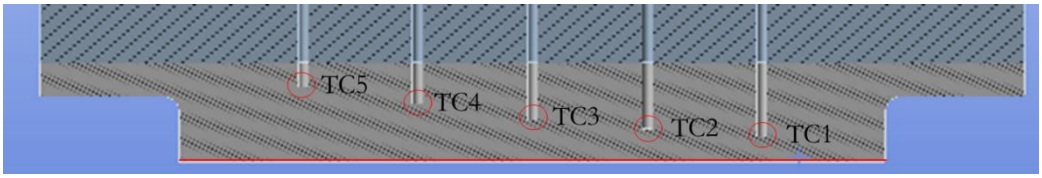

Figure 18. Thermocouple map for the first round

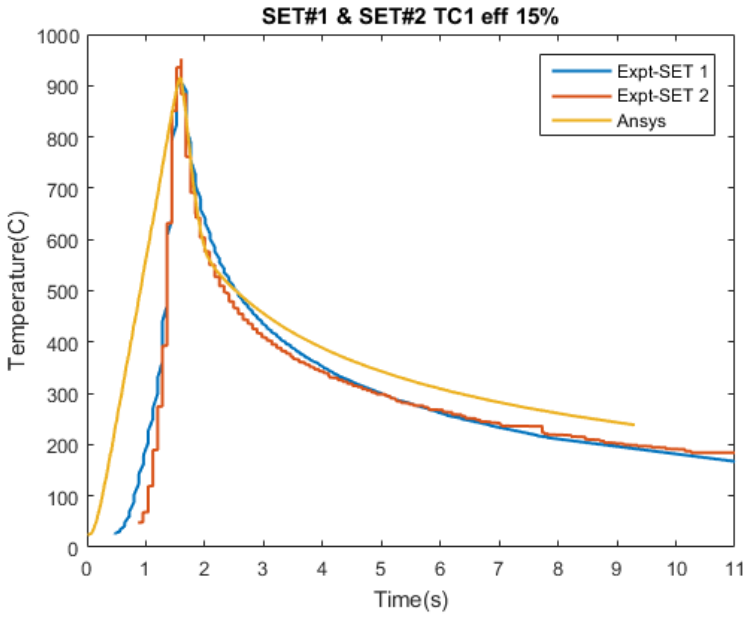

Figure 19. TC1 (thermocouple), temperature profile comparison

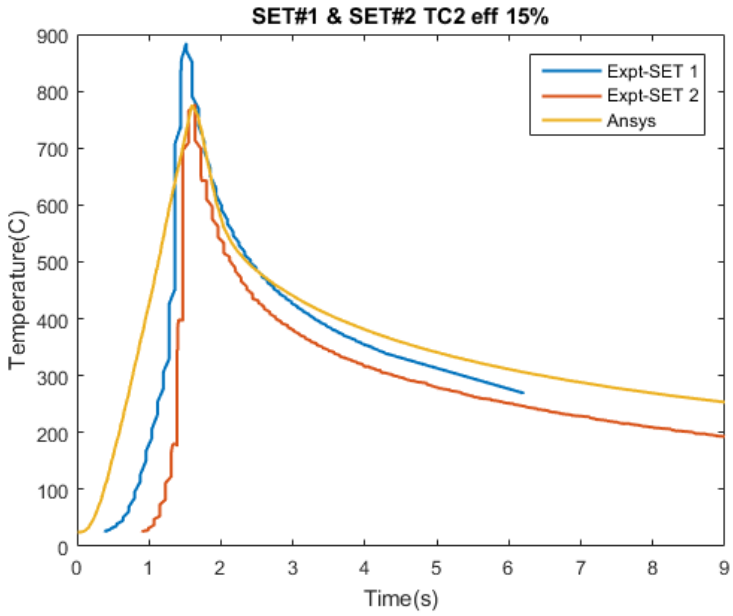

Figure 20. TC2 (thermocouple), temperature profile comparison

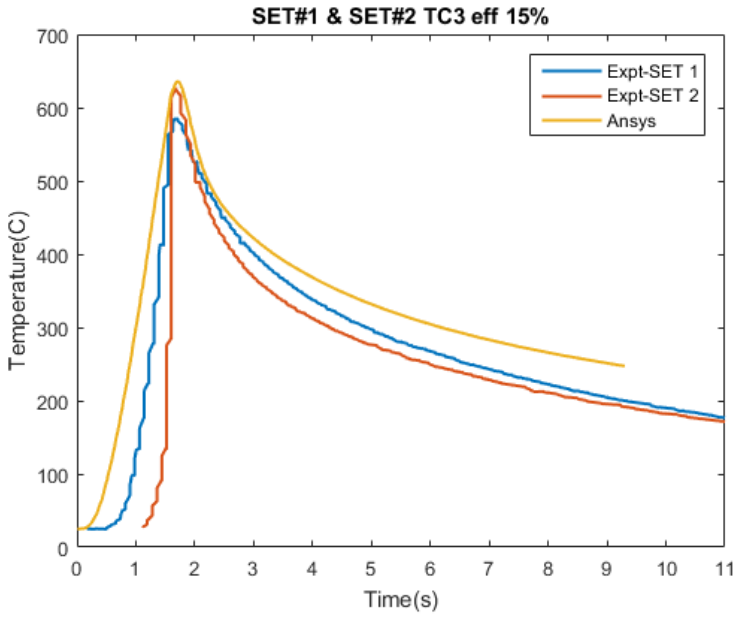

Figure 21. TC3 (thermocouple), temperature profile comparison

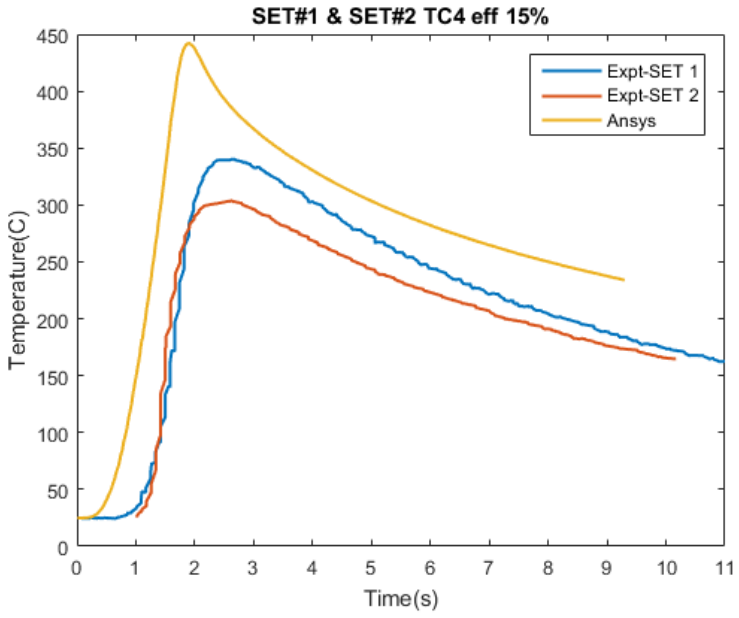

Figure 22. TC4 (thermocouple), temperature profile comparison

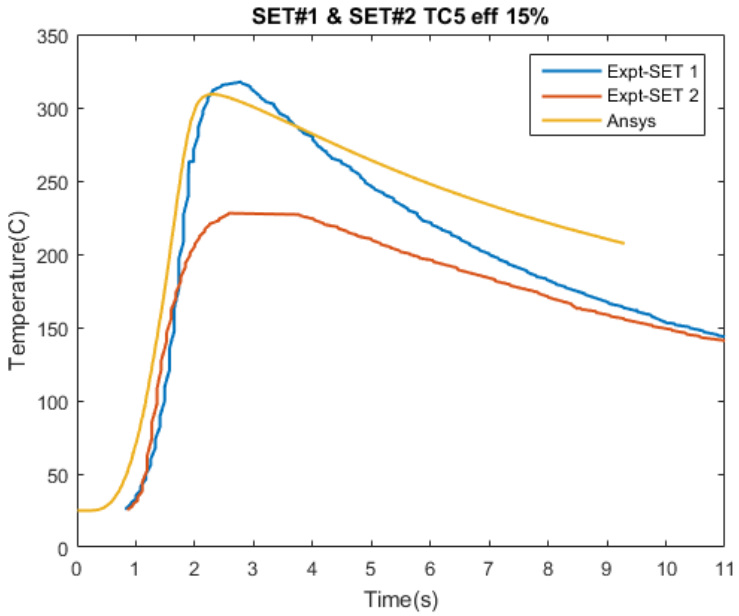

Figure 23. TC5 (thermocouple), temperature profile comparison

A good agreement between experimental and simulation components is observed at 15% efficiency with the exception of Thermocouple 4.

The comparison between temperature profiles from experiments and simulations at various thermocouple positions; see Figure 19 - Figure 23, show a disconnect between experimental measurements from set 1 and set 2. Disconnect in between measured temperature profiles from each set could be the result of either one being a faulty thermocouple.

Furthermore, it is observed that a few of the measured temperature profiles are incorrect as no common trend is established among coupons of equal interface surface area. With temperature profiles for similar interface surface areas varying widely. In case of TC 1, 2 and 3, the variation could be explained due to the thermocouples burned off, as they are positioned close to the interface. Due to which the measured temperature profile for TC 1, 2 and 3 is inaccurate. Variation between the temperature profile is also discovered in the case of TC 5; see Figure 24, even though TC 5 is at a safe distance from the interface to prevent being burned off.

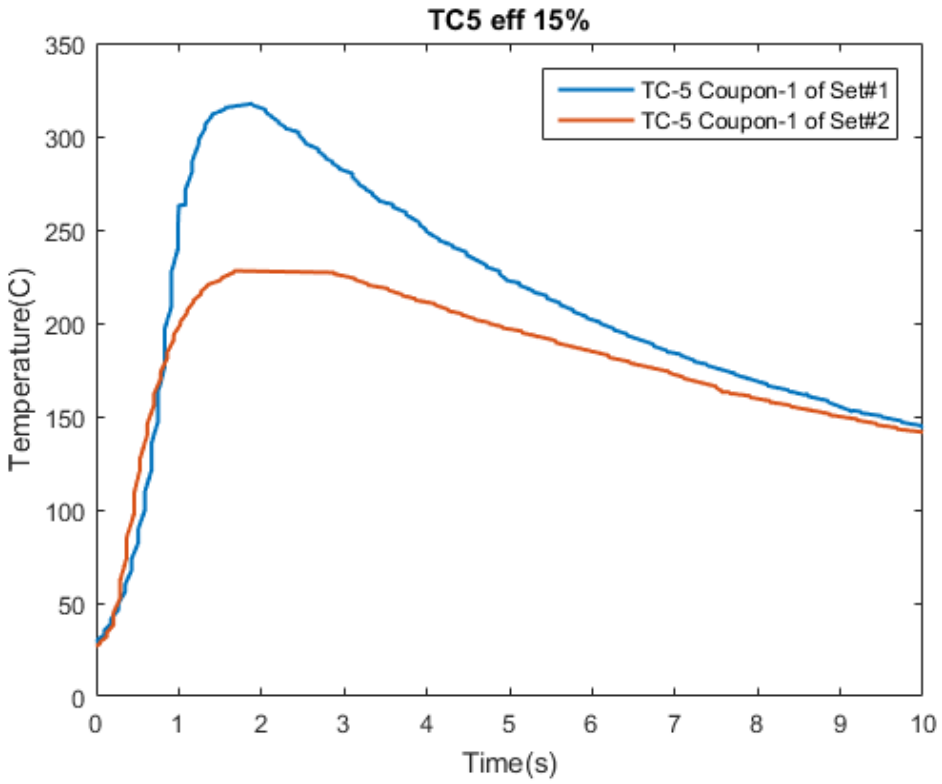

Figure 24. Comparison of TC-5 temperature profile measurements from each Set

Identical interface surface area generates an equal amount of frictional heat when subjected to common relative motion. Two coupons have equal interface surface area across set 1 and set 2 are taken into consideration for Figure 24 and temperature profile of TC 5 is compared.

Variation between temperature profiles in case of TC 4 and TC 5 can be due to either thermocouple inefficiency or due to poor connection between the thermocouple and the coupon.

The farthest thermocouple produces the most dependable experimental thermal data provided the connection is proper.

3.2 Experimental model revision

Due to Thermocouples placement with respect to the interface; see Figure 18, they were often burned during welding. Resulting in discrepancies in the experimentally recorded temperature profiles across different coupons. The thermocouple inefficiency might also have added to the discrepancy in the experimental thermal measurements of different thermocouples.

To gain fairly accurate temperature profiles from experiments and avoid incorrect measurements, thermocouple positions were altered; see Figure 25. All thermocouple positions are set far enough from the interface to avoid any burnout. Thermocouple positions, TC 1-5 are defined to study the temperature variation across interface at a similar depth. While TC 6 is solely focused on temperature profile calibration.

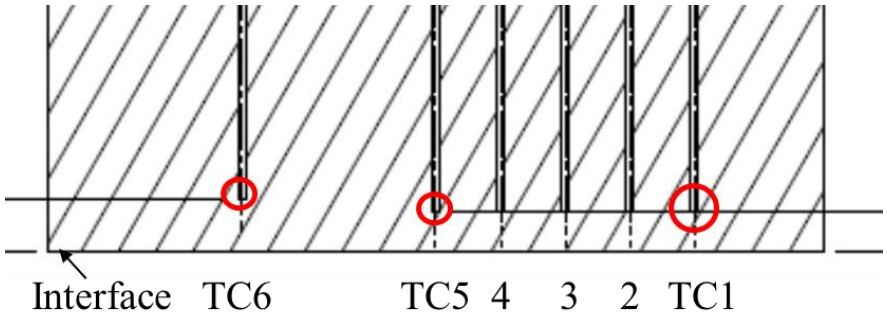

Figure 25. Redesigned Thermocouple Map for the second round

3.3 Mathematical model revision

3.3.1 Implementation of interface displacement

During the OFW welding, the interface is displaced through the process. The interface displacement is a result of frictional force and forging force applied. The interface displacement is one of the monitored parameters; see Figure 26.

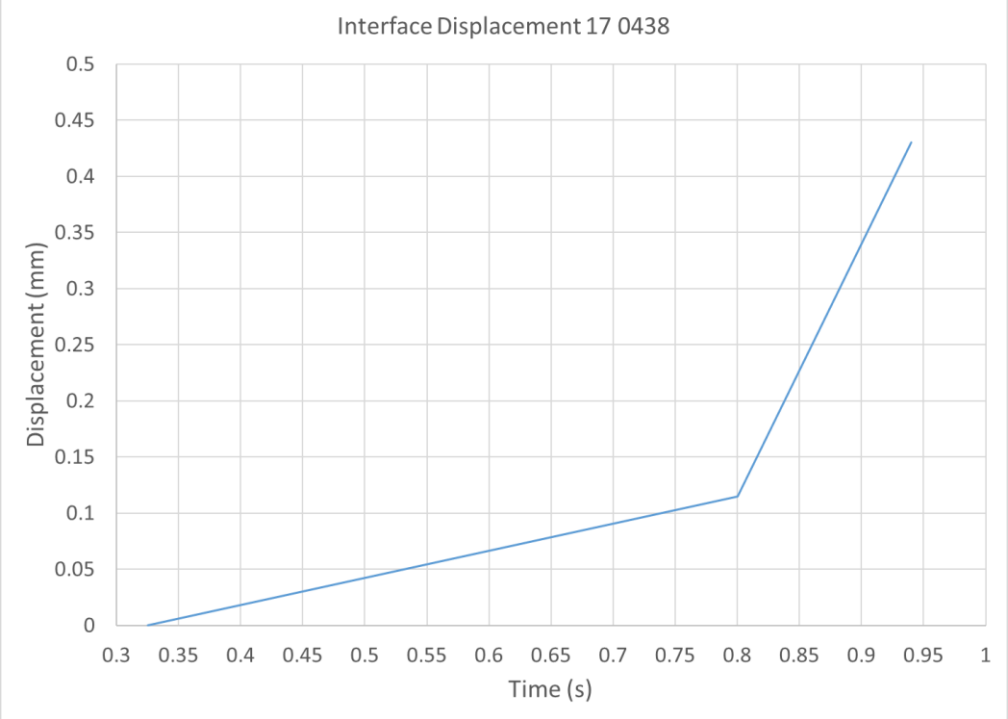

Figure 26. Interface Displacement with respect to time

Interface displacement begins early in the OFW process as a high volume of heat is generated due to frictional force. Displacement increases gradually till the coupons are realigned. Once coupons are realigned and forging force is applied the interface displacement increases drastically; see Figure 26 and Figure 27.

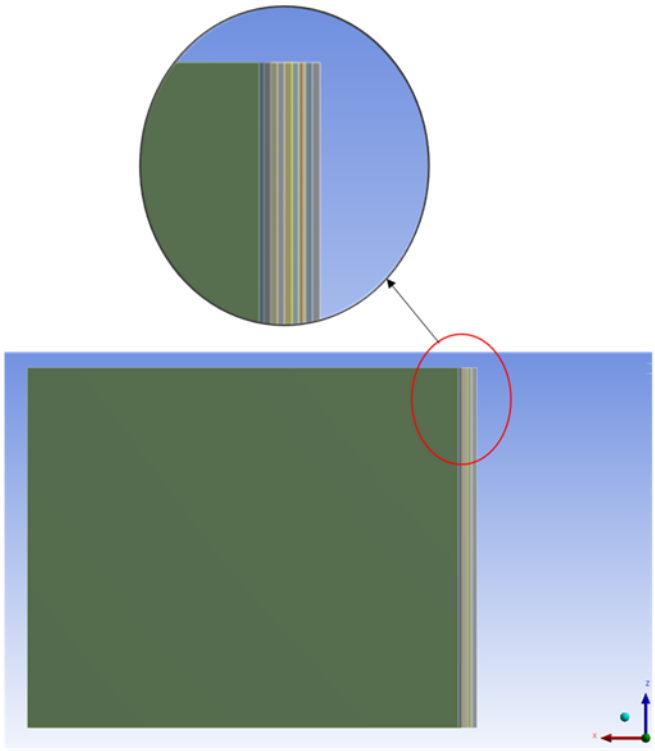

Interface Step no.	Displacement (mm)	Time (s)
1	0	0.325
2	0.05	0.53152
3	0.1	0.73804
4	0.115	0.8
Linear Break		
5	0.115	0.8
6	0.15	0.81556
7	0.2	0.83778
8	0.25	0.86
9	0.3	0.88222
10	0.35	0.90444
11	0.4	0.92667
12	0.43	0.94

Layers are divided every 0.05 mm of displacement.

Figure 27. Interface displacement incorporated in a mathematical model

The mathematical model was redesigned to incorporate the interface displacement; see Figure 27. Taking interface displacement into consideration for every 0.05 mm, a new layer is formed. Heat flux is broken down to be applied for every 0.05 mm, and the remainder of the heat flux is applied to the last layer; see Figure 28. As the interface advances the previous layer dissipates heat while keeping the coupon volume constant.

The linear break exhibited in Figure 27 is the point when coupons are realigned to coincide and the forging force is applied.

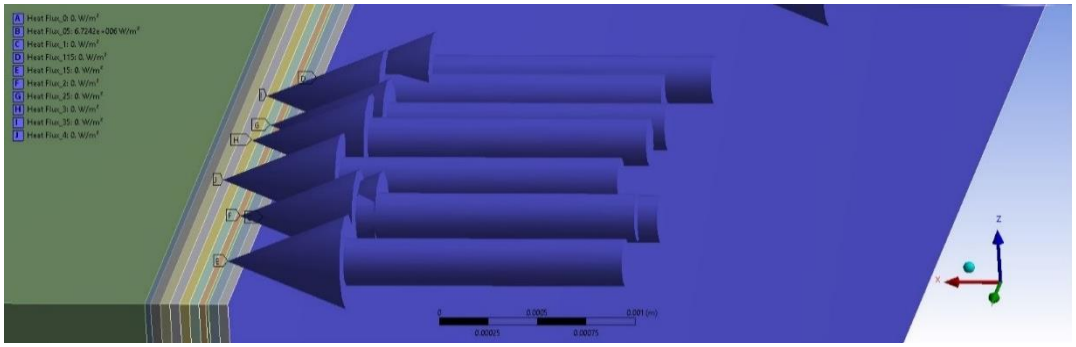

Figure 28. Heat Flux Applied to respective layers

The aim of heat flux applied to the varying interface is to study the difference in approximations calculated from a constant and a varying interface. While a sequential thermal to structural simulation is possible in ANSYS a coupled simulation is still not possible. By varying the interface in a transient thermal simulation a pseudo-interface displacement is generated.

Previously heat flux was applied to a constant interface over time; see Figure 13, without taking interface displacement into consideration. Approximations of temperature profiles at various thermocouple positions calculated through simulations will vary as the heat flux is applied to a varying interface.

3.3.2 Redefining frictional heat flux

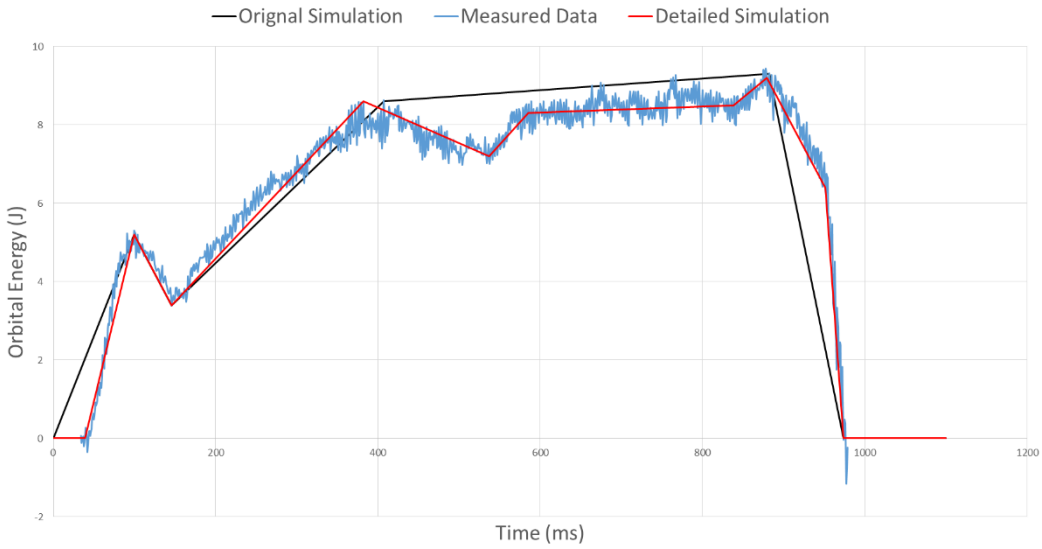

Figure 29. Orbital Energy vs Time

There is a certain amount of uncertainty regarding the efficiency factor determined by utilizing electrical power consumption recorded during experiments, as a major portion of power is depleted post its measurement and before the point where welding initiates.

For more accurate efficiency factor, orbital energy is computed from recorded motion orbital torque and piston pressure, both are monitored process parameters. Calculated orbital energy is broken down into load steps to be used as Heat flux input for the mathematical model; see Figure 29.

Chapter 4

Results

Introduction – the second round of coupons

The second round of coupons includes a total of ten orbital friction welded joints. These ten joints are classified based on the interface surface are of coupons being welded. Coupons with the interface surface area of 250 mm², 480 mm², and 800 mm² are welded by OFW process in the second round of welding; see Figure 30.

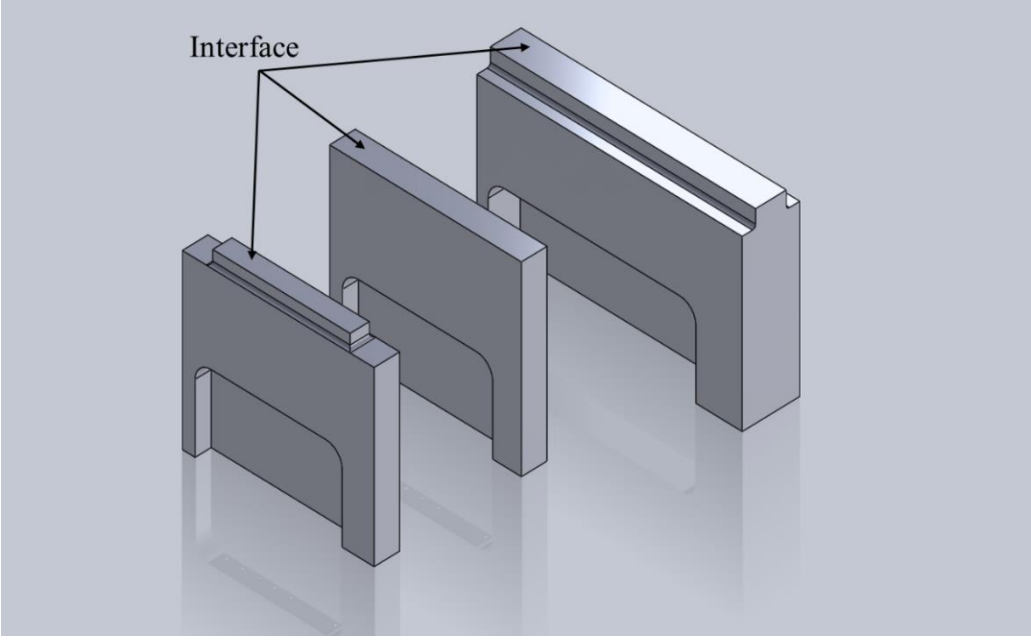

Figure 30. Coupons classified based on interface surface area.

Ten joints consist of three sets of each 250 mm² and 800 mm² coupons and four sets of 480 mm² coupons. The objective is to observe the variation in efficiency factor across the sets with equal interface surface area and across increasing interface surface area.

In regard to the mathematical model for the second round of coupons, the heat flux is derived from the calculated Orbital Energy applied during OFW process. Also, Heat flux application is coupled with interface displacement to compensate for movement in interface during OFW process and to take into consideration the heat loss due to flash. Heat loss due to conduction, convection, and radiation are applied according to initial boundary conditions.

Following Results are divided into three zones based on interface surface area starting with 250 mm². Results show graphs of temperature profiles from simulations carried out using ANSYS calibrated to thermocouple recordings from experiments. Also, exhibiting the efficiency factors employed to calibrate the simulation temperature profiles to the experimental measurements.

For reference thermocouple map used during welding of the second round of coupons for all the ten sets is provided; see Figure 31.

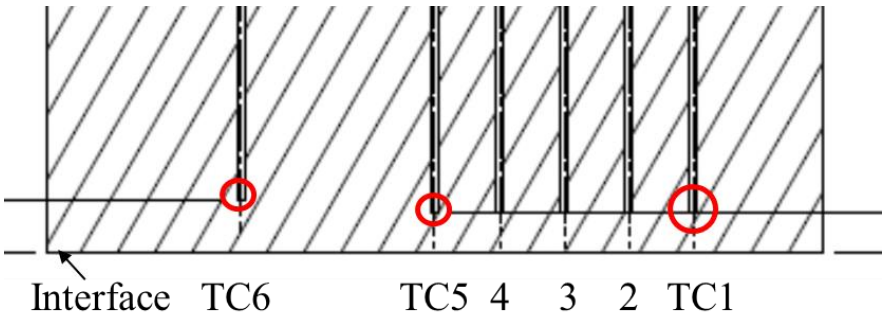

Figure 31. Thermocouple map for second round of coupons

Results - 250 mm² coupons

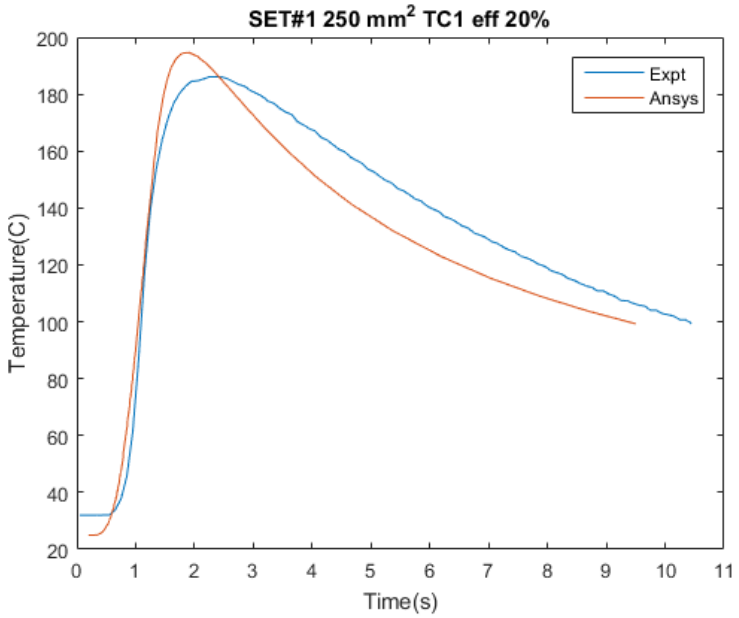

Figure 32. SET-1 250 mm², TC-1 temperature profile comparison

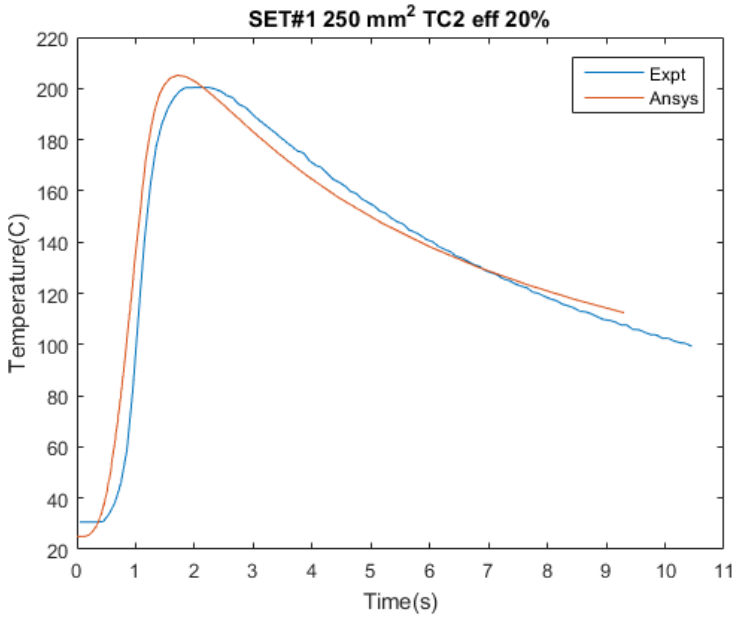

Figure 33. SET-1 250 mm², TC-2 temperature profile comparison

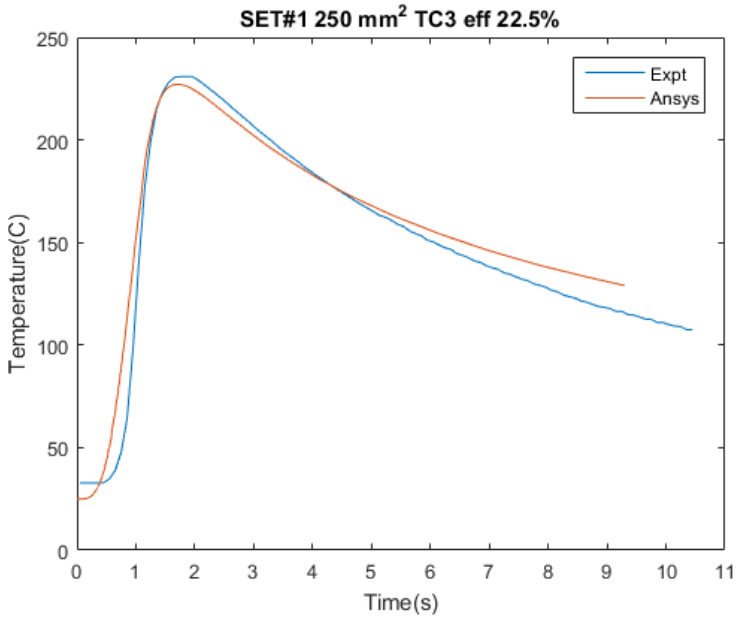

Figure 34. SET-1 250 mm², TC-3 temperature profile comparison

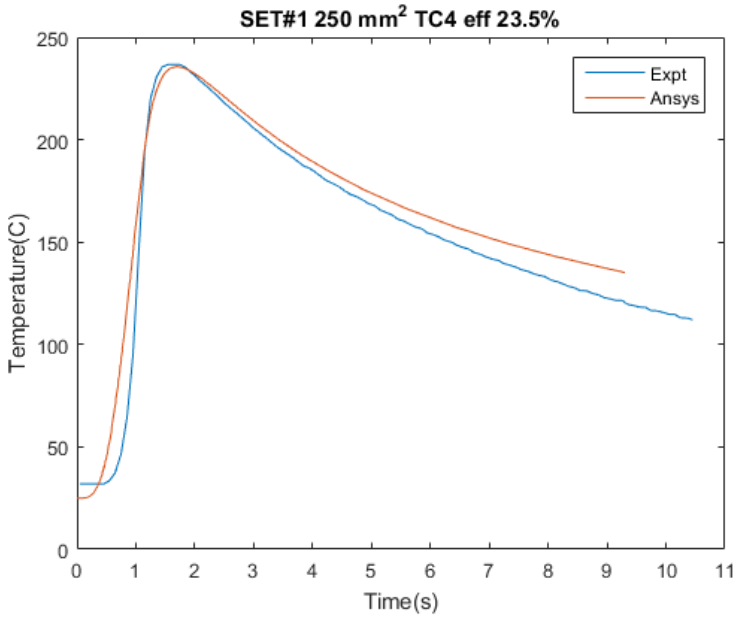

Figure 35. SET-1 250 mm², TC-4 temperature profile comparison

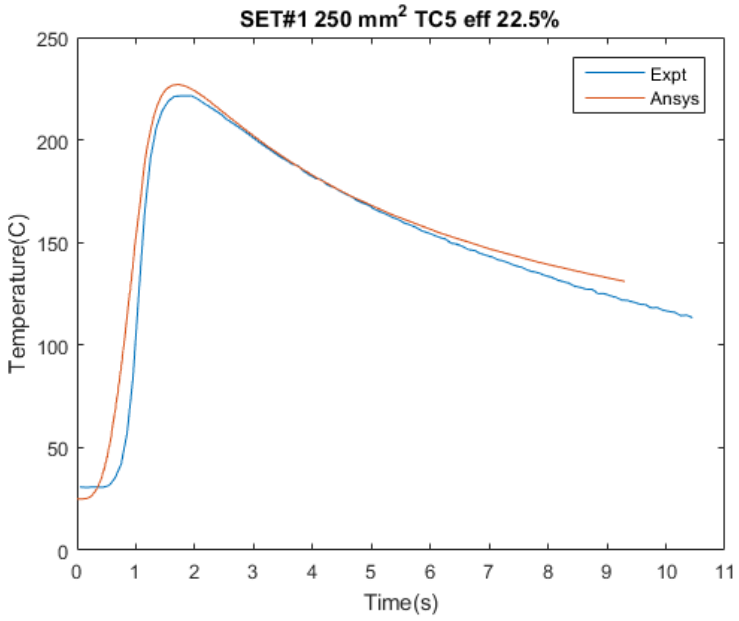

Figure 36. SET-1 250 mm², TC-5 temperature profile comparison

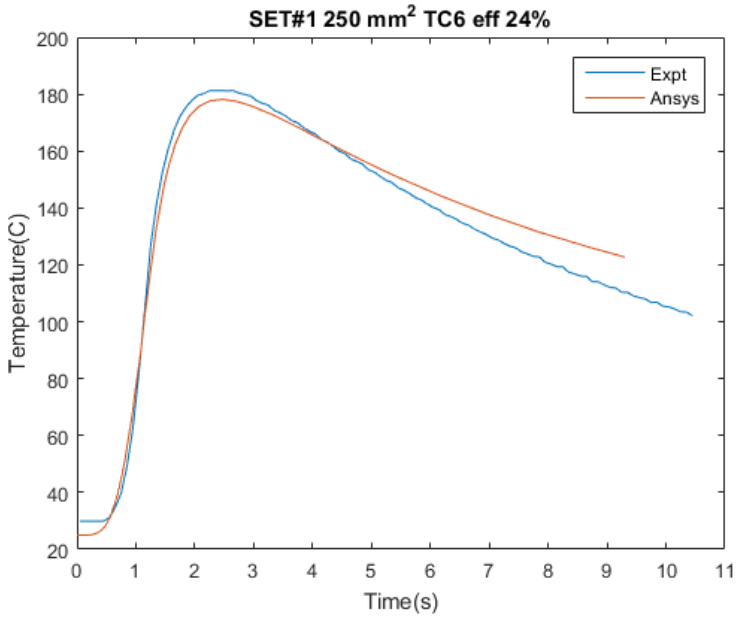

Figure 37. SET-1 250 mm², TC-6 temperature profile comparison

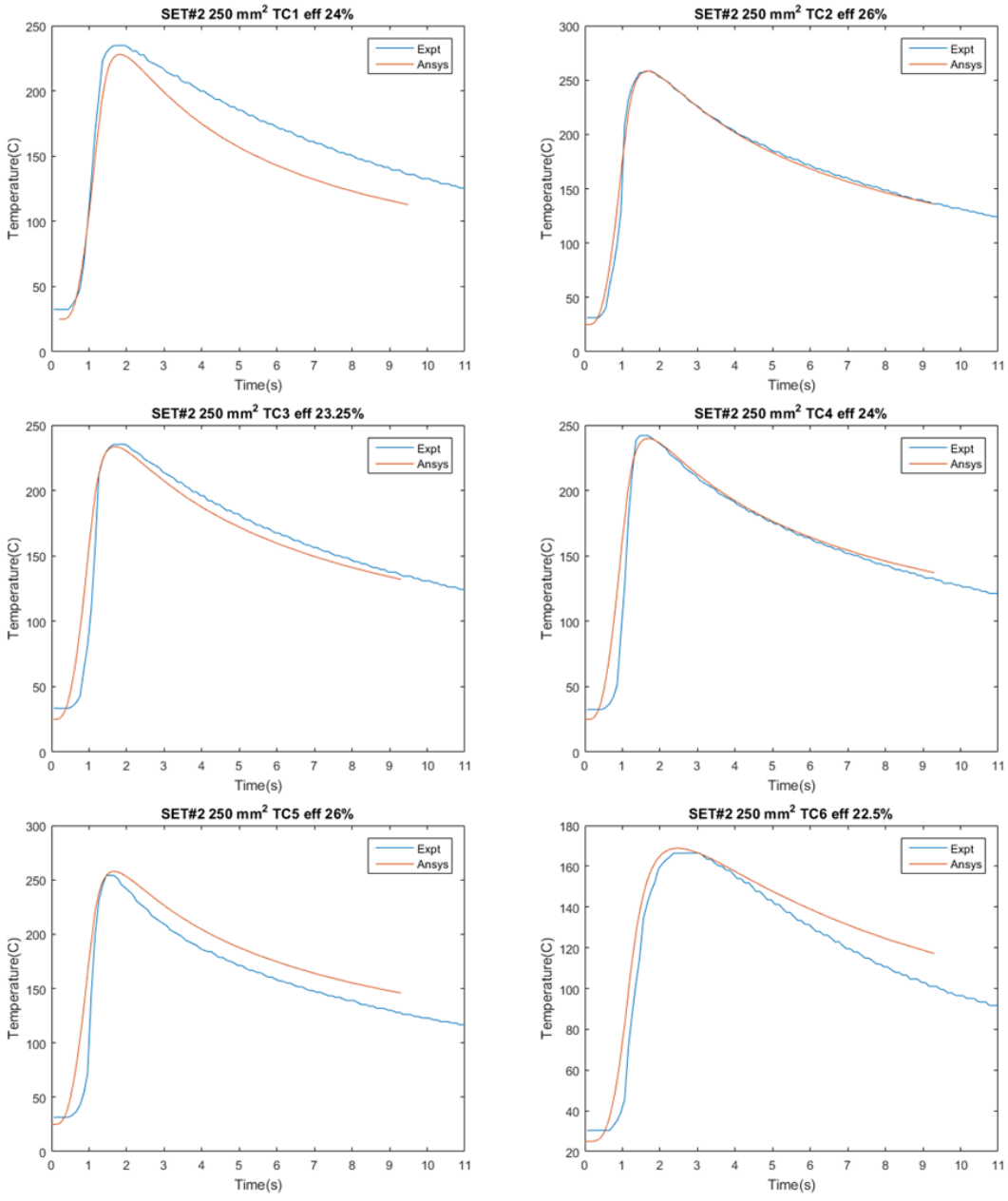

Figure 38. SET – 2 250 mm², TC 1-6 temperature profile comparison

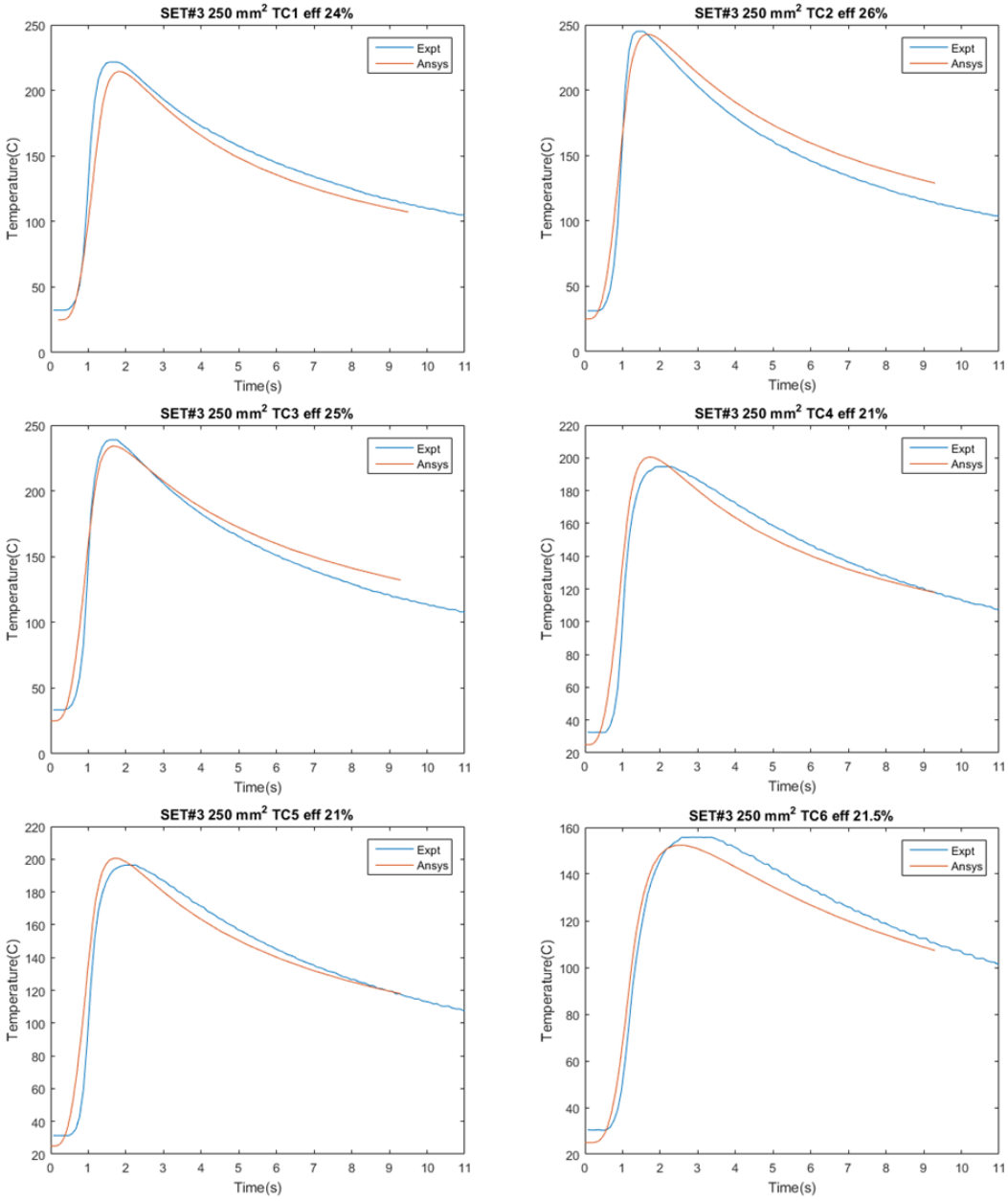

Figure 39. SET – 3 250 mm², TC 1-6 temperature profile comparison

250 mm²	Efficiency Factors		
	SET-1	SET-2	SET-3
TC-1	20	24	24
TC-2	20	26	26
TC-3	22.5	23.25	25
TC-4	23.5	24	21
TC-5	22.5	26	21
TC-6	24	22.5	21.5
Average	22.08	24.29	23.08
Standard Deviation	1.72	1.44	2.20

Figure 40. Efficiency factors for 250 mm² Sets

For coupons with interface surface area 250 mm², efficiency factors for each thermocouple and temperature profile comparisons between simulations and experiments for all the three sets are exhibited. For the set - 1 from Figure 32 - Figure 37, for the set – 2; see Figure 38, and for the set – 3; see Figure 39.

Good agreement between calculated and experimental thermocouple profiles is observed. As expected efficiency across interface varies. Calibration of thermocouples placed at the same depth across interface produces a range of efficiencies; see Figure 40. Average and standard deviation for each set are calculated; see Figure 40.

The efficiency factors listed for each set are utilized to draw a box plot to demonstrate the trend in maximum, minimum and median efficiencies across coupons with similar interface surface area; see Figure 41.

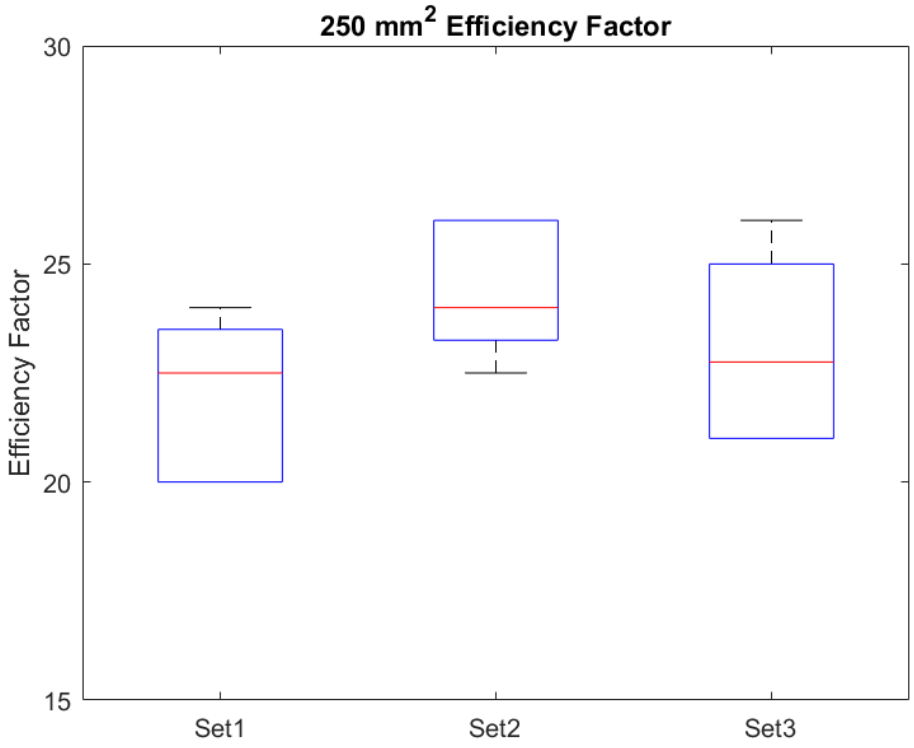

Figure 41. Box Plot of Efficiency Factors of 250mm² sets

Redline in each box plot represents the median of efficiency factors from that particular set. While the box itself and the extension show the range of efficiency factors for the set in consideration. The efficiency factors within the range of 20% - 26% without any outliers are achieved. Consistent efficiency factors are predicted for 250 mm² area coupons based on 18 thermocouple data set.

The numerical model is utilized to predict temperature profiles across interface and temperature flow through the coupons with the interface surface area of 250 mm².

Results – 480 mm² coupons

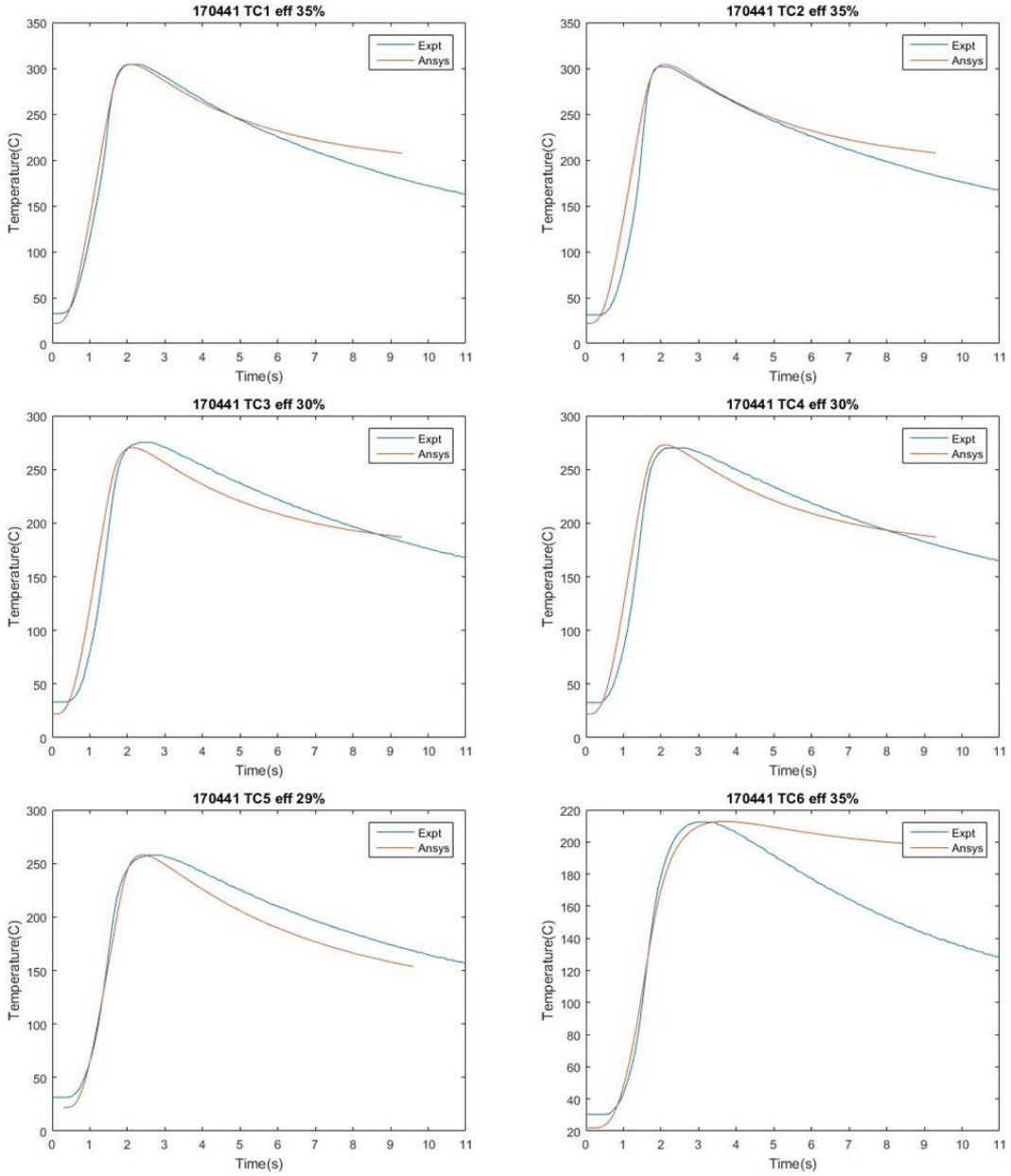

Figure 42. SET – 6 480 mm², TC 1-6 temperature profile comparison

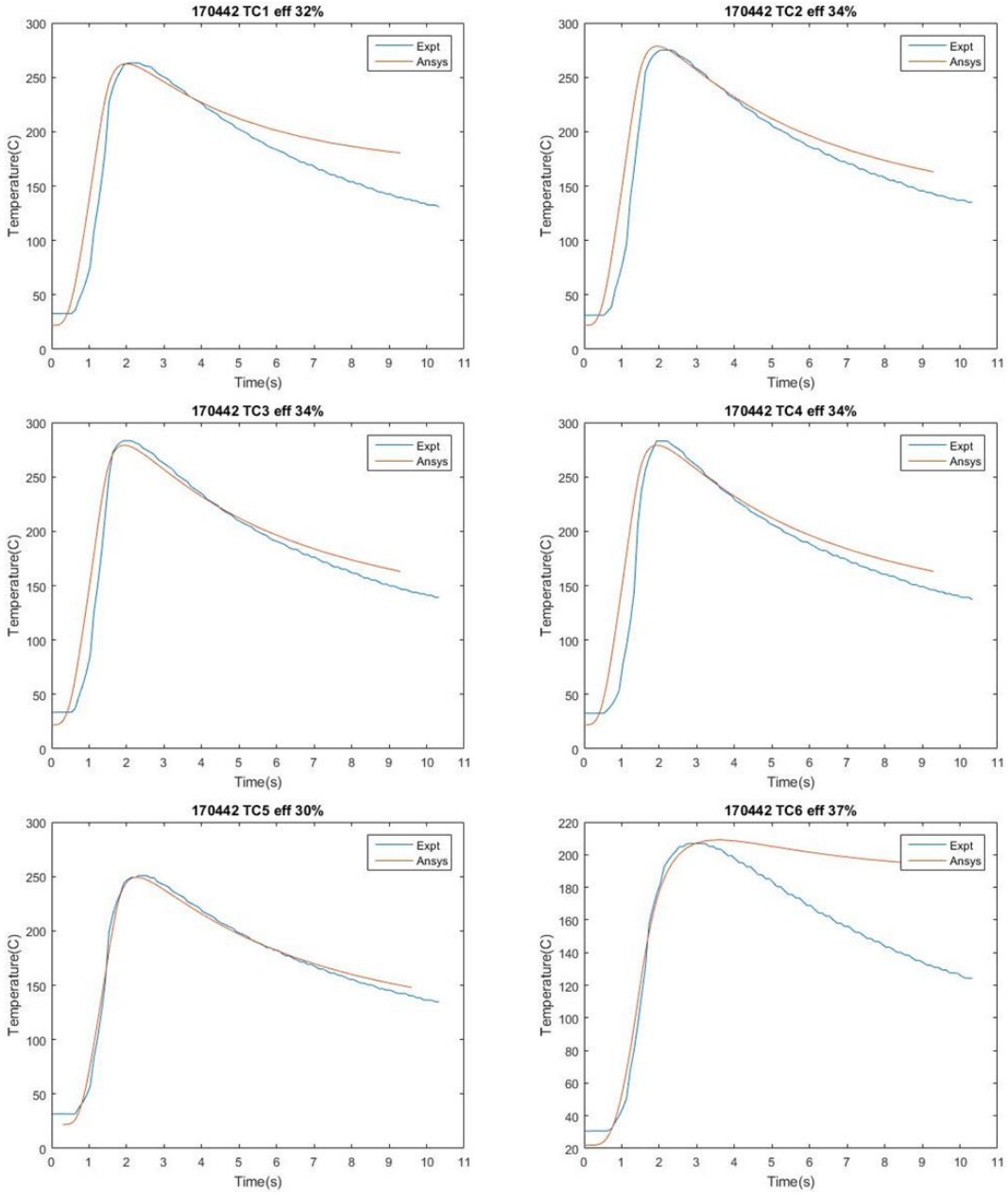

Figure 43. SET – 7 480 mm², TC 1-6 temperature profile comparison

480 mm²	Efficiency Factors			
	SET-4	SET-5	SET-6	SET-7
TC-1	25	33	35	32
TC-2	35	27	35	34
TC-3	31	30	30	34
TC-4	33	30	30	34
TC-5	35	38	29	30
TC-6	25	36	35	37
Average	30.67	32.33	32.33	33.50
Standard Deviation	4.63	4.13	2.94	2.35

Figure 44. Efficiency factors for 480 mm² Sets

For coupons with interface surface area 480 mm², efficiency factors for each thermocouple and temperature profile calculations for all four sets, set 4 - 7 are carried out utilizing ANSYS. Temperature profile comparison between simulations and experiments is exhibited. For the set - 6; see Figure 42, for the set – 7; see Figure 43.

Good agreement between calculated and experimental thermocouple profiles is observed. As expected efficiency across interface varies. Calibration of thermocouples placed at the same depth across interface produces a range of efficiencies; see Figure 44. Average and standard deviation for each set are calculated; see Figure 44.

The efficiency factors listed for each set are utilized to draw a box plot to demonstrate the trend in maximum, minimum and median efficiencies across coupons with similar interface surface area; see Figure 45.

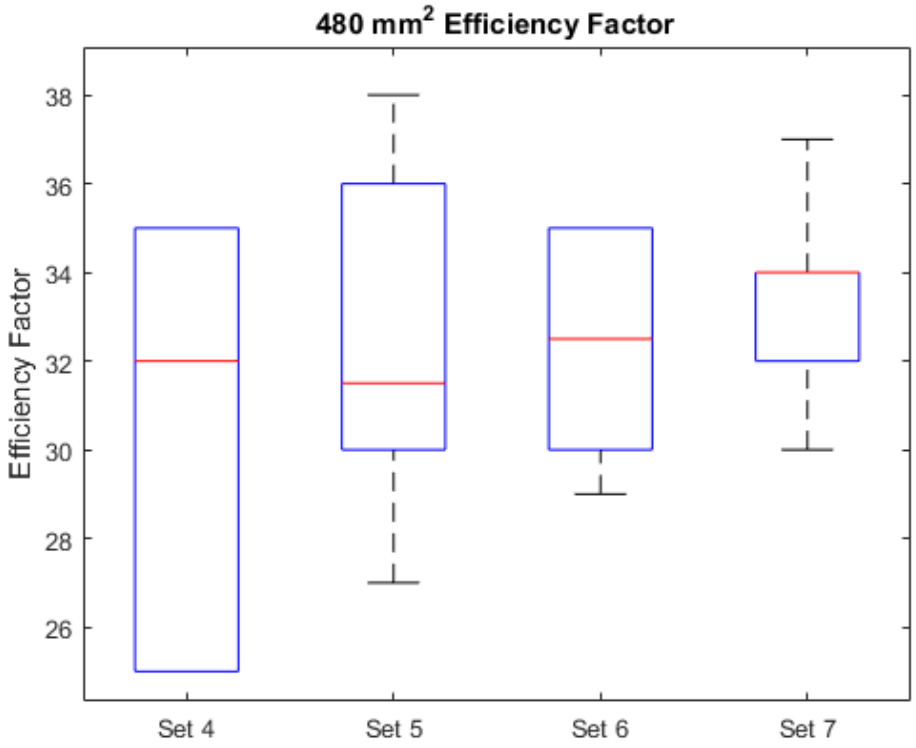

Figure 45. Box Plot of Efficiency Factors of 480mm² sets

The efficiency factors for 480 mm² coupons have a wider range as compared to 250 mm² resulting in higher error estimate during approximation through the mathematical order. Average efficiency factors for 480 mm² lie within the range of 30.6 % - 33.5 %. Consistent average efficiency factors are predicted for 480 mm² area coupons based on 24 thermocouple data set.

The numerical model is utilized to predict temperature profiles across interface and temperature flow through the coupons with the interface surface area of 480 mm².

Results – 800 mm² coupons

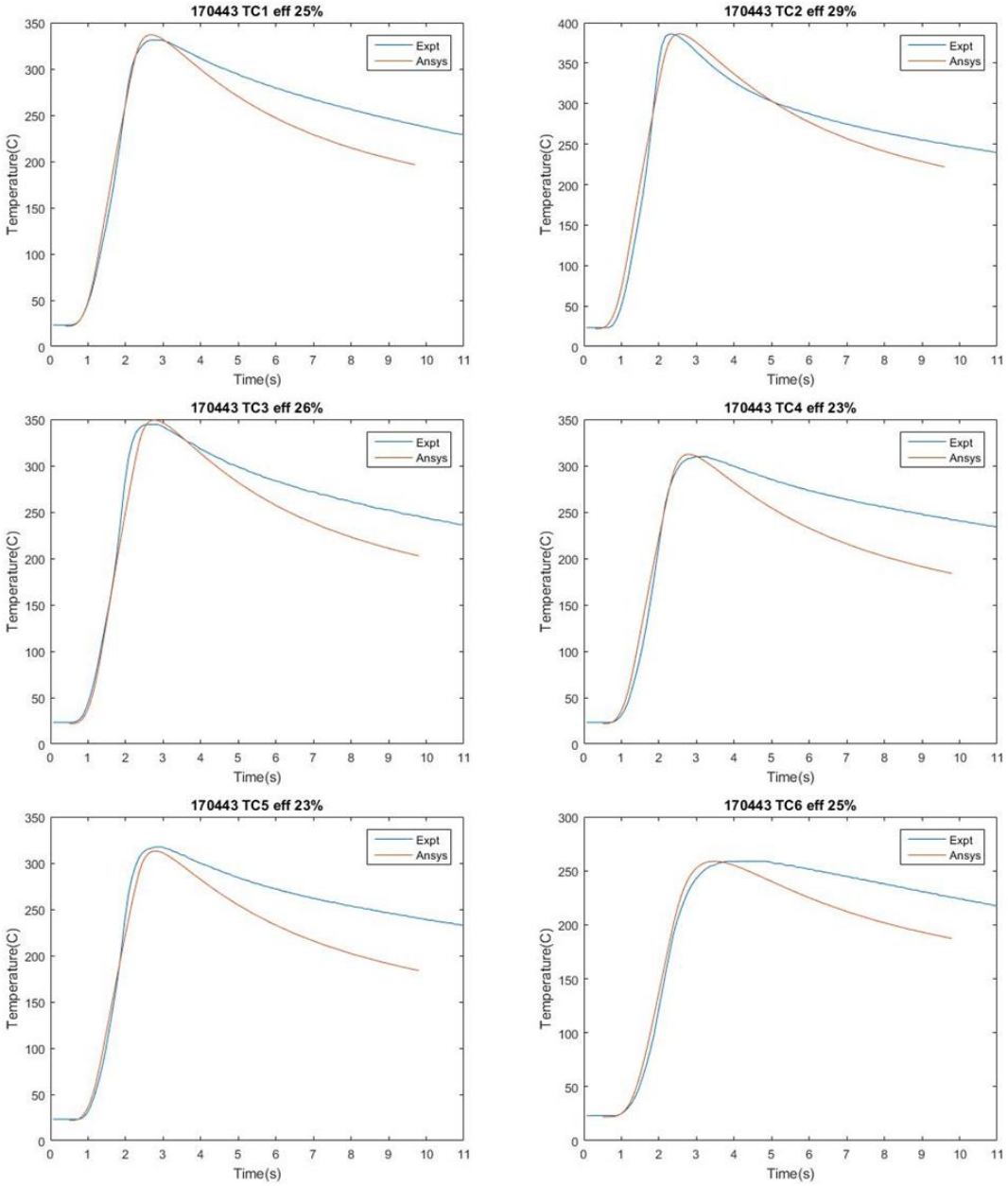

Figure 46. SET – 8 800 mm², TC 1-6 temperature profile comparison

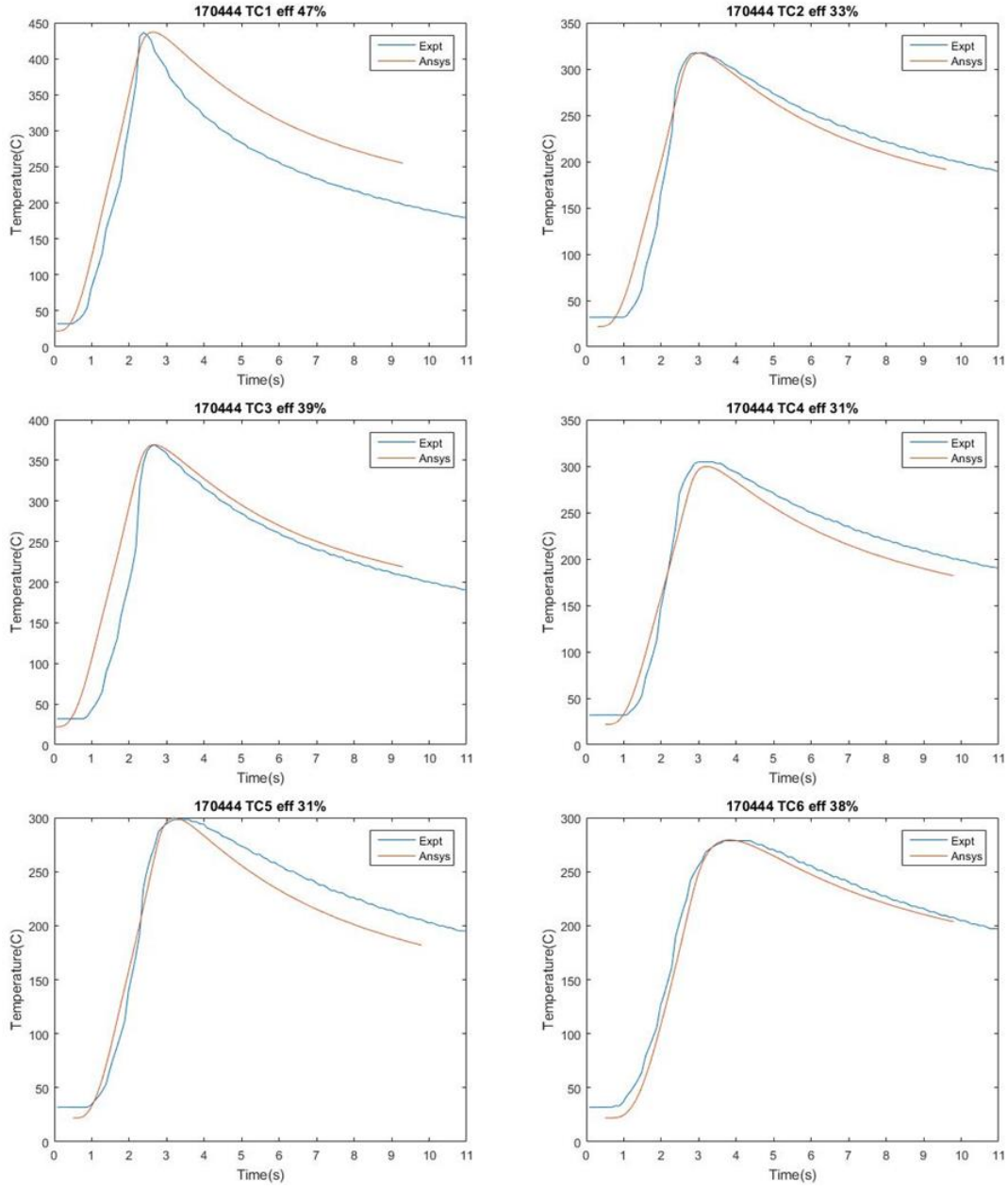

Figure 47. SET – 9 800 mm², TC 1-6 temperature profile comparison

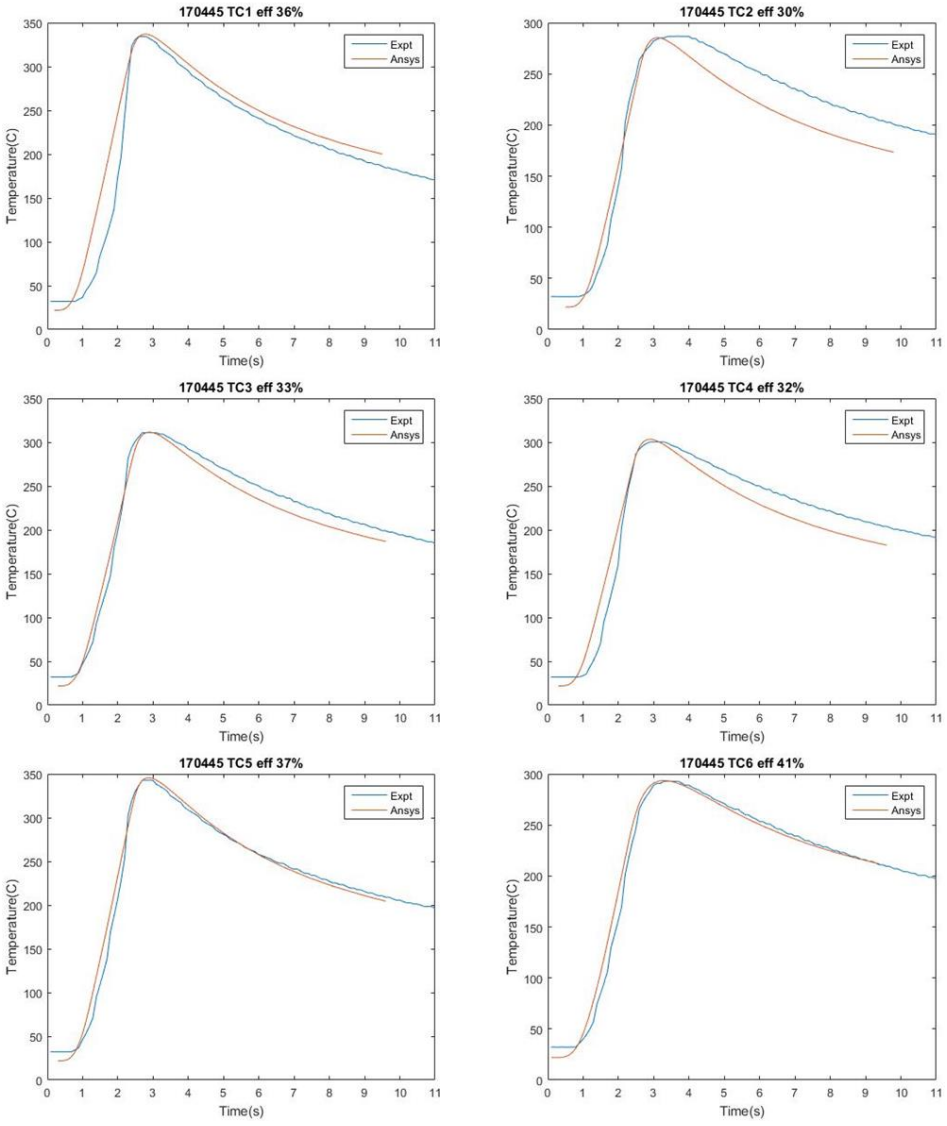

Figure 48. SET – 10 800 mm², TC 1-6 temperature profile comparison

800 mm²	Efficiency Factors		
	SET-8	SET-9	SET-10
TC-1	25	47	36
TC-2	29	33	30
TC-3	26	39	33
TC-4	23	31	32
TC-5	23	31	37
TC-6	25	38	41
Average	25.17	36.50	34.83
Standard Deviation	2.23	6.19	3.97

Figure 49. Efficiency factors for 800 mm² Sets

For coupons with interface surface area 800 mm², efficiency factors for each thermocouple and temperature profile comparisons between simulations and experiments for all the three sets are exhibited. For the set - 8; see Figure 46, for the set - 9; see Figure 47, and for the set – 10; see Figure 48.

Good agreement between calculated and experimental thermocouple profiles is observed. As expected efficiency across interface varies. Calibration of thermocouples placed at the same depth across interface produces a range of efficiencies; see Figure 49. Average and standard deviation for each set are calculated; see Figure 49.

The efficiency factors listed for each set are utilized to draw a box plot to demonstrate the trend in maximum, minimum and median efficiencies across coupons with similar interface surface area; see Figure 50.

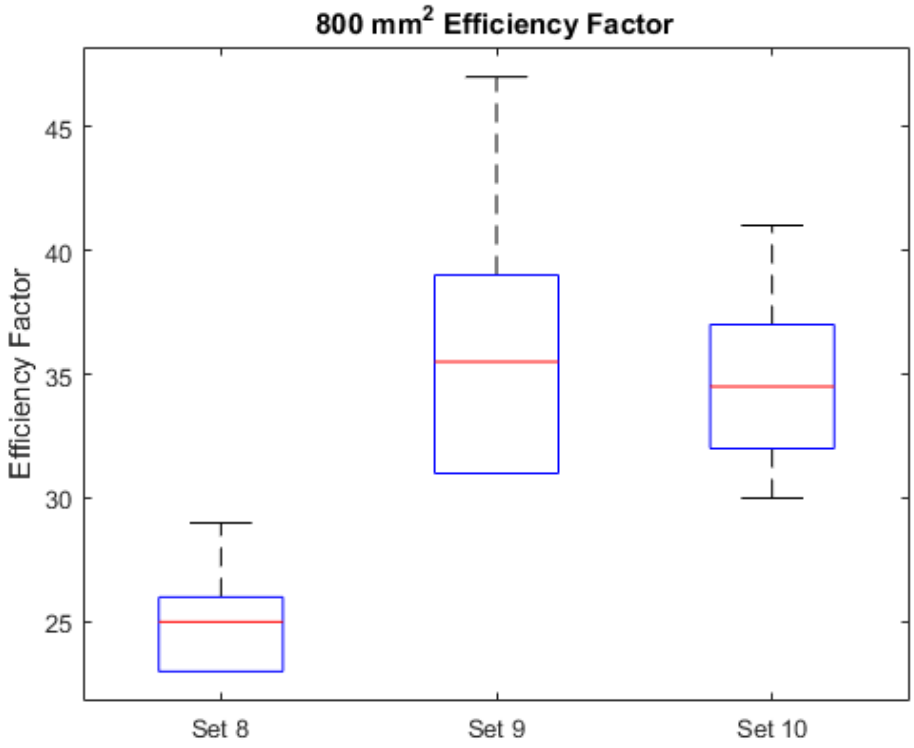

Figure 50. Box Plot of Efficiency Factors of 800mm² sets

The efficiency factors for 800 mm² coupons have a wider range as compared to 480 mm² and 250 mm² resulting in higher error estimate during approximation through the mathematical order. In the case of 800 mm² coupons the main cause of upset is set - 8. While average efficiency factors are consistent for set - 9 and set - 10 for 800 mm².

The heat flux input provided for all mathematical models in round 2 of welding is derived from orbital energy calculated from process parameters. Heat flux input for the mathematical model in all three sets of 800 mm² coupons is provided; see Figure 51.

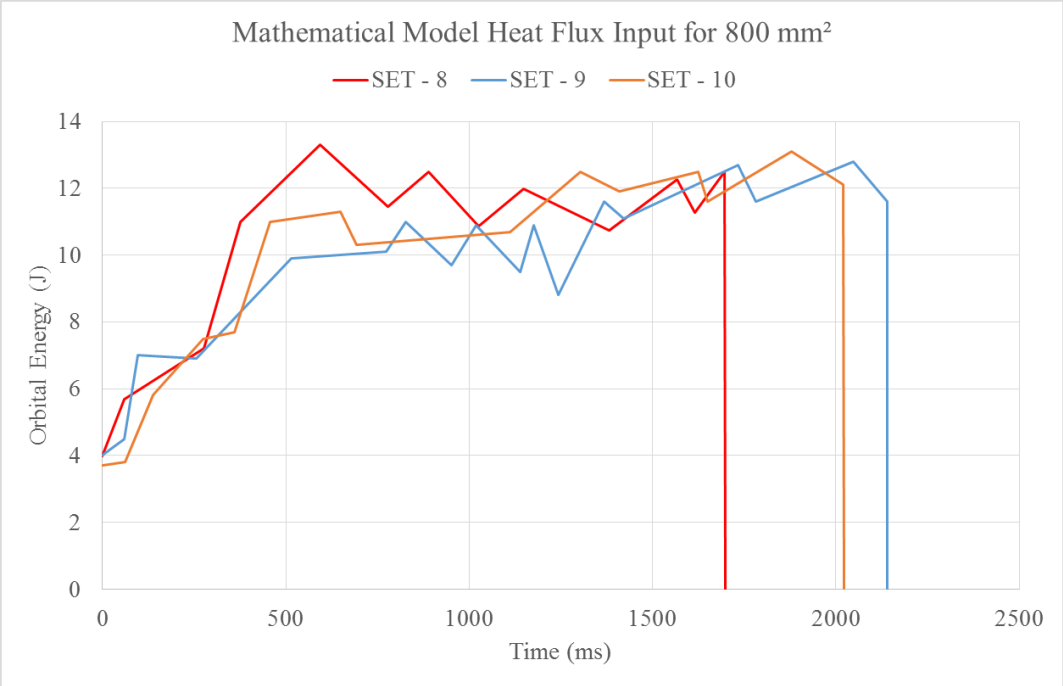

Figure 51. Comparison of heat flux input across 800 mm² sets

For set - 8, heat flux is applied up to 1.7 seconds while for set - 9 and set - 10 the heat flux is applied beyond 2 seconds; see Figure 51. The volume of frictional heat generated for the set - 8 will be lesser as compared to set - 9 and set - 10. For set - 9 or set - 10 higher volume of heat is applied which results in higher temperature measurements taken from thermocouples. Calibrating efficiency factor with higher temperature results in higher efficiency of set - 9 and set - 10.

A thermal transient model for efficiency calibration is developed taking conduction, convection, and radiation heat loss into account. Also taken into account is the interface displacement by flash extrusion due to frictional welding force and forging force applied during the orbital frictional welding process.

Chapter 5

Conclusion

On the basis of analytical and numerical modeling of orbital frictional welding of Ti6Al4V components following points were concluded:

The developed computational model

- considers the variation in material properties with the variation in temperature.
- calculates the temperature profile at any point throughout the orbital frictional welding process.
- produces an efficiency factor based on temperature profile calibration.
- takes into consideration the formation of flash and the interface displacement occurring during the process while calculating the temperature profile.
- takes into consideration the heat losses to the surroundings.

References

[1] A. Vairis and M. Frost, “High frequency linear friction welding of a titanium alloy,” *Wear*, vol. 217, no. 1, pp. 117–131, Apr. 1998.

[2] M. Maalekian and H. Cerjak, “Modelling the orbital friction welding of pearlitic steel bars,” *ASM Proc. Int. Conf. Trends Weld. Res.*, pp. 736–741, 2009.

[3] A. R. Mcandrew, P. A. Colegrove, C. Bühr, B. C. D. Flipo, and A. Vairis, “A literature review of Ti-6Al-4V linear friction welding,” 2018.

[4] P. Wanjara and M. Jahazi, “Linear friction welding of Ti-6Al-4V: Processing, microstructure, and mechanical-property inter-relationships,” *Metall. Mater. Trans. A*, vol. 36, no. 8, pp. 2149–2164, Aug. 2005.

[5] “Rotary Friction Welding - Job Knowledge 148.” [Online]. Available: https://www.twi-global.com/technical-knowledge/job-knowledge/rotary-friction-welding-148/. [Accessed: 11-Apr-2018].

[6] U. Raab, S. Levin, L. Wagner, and C. Heinze, “Orbital friction welding as an alternative process for blisk manufacturing,” *J. Mater. Process. Technol.*, vol. 215, no. 1, pp. 189–192, 2015.

[7] “ANSYS® Academic Research Mechanical, Release 18.1.” ANSYS, Inc.,

2018.

[8] R. Boyer, G. Welsch, and E. W. Collings, *Materials properties handbook : titanium alloys*. ASM International, 1994.

[9] J. Sorina-Müller, M. Rettenmayr, D. Schneefeld, O. Roder, and W. Fried, "FEM simulation of the linear friction welding of titanium alloys," *Comput. Mater. Sci.*, vol. 48, no. 4, pp. 749–758, Jun. 2010.

[10] *ANSYS Theory Refrence Release 5.6*. ANSYS; Inc., 1999.

[11] M. Maalekian, E. Kozeschnik, H. P. Brantner, and H. Cerjak, "Comparative analysis of heat generation in friction welding of steel bars," *Acta Mater.*, vol. 56, no. 12, pp. 2843–2855, Jul. 2008.

[12] R. Turner, J.-C. Gebelin, R. M. Ward, and R. C. Reed, "Linear friction welding of Ti–6Al–4V: Modelling and validation," *Acta Mater.*, vol. 59, no. 10, pp. 3792–3803, Jun. 2011.

[13] A. Vairis and M. Frost, "Modelling the linear friction welding of titanium blocks," *Mater. Sci. Eng. A*, vol. 292, no. 1, pp. 8–17, Nov. 2000.

[14] R. E. Craine and A. Francis, "Frictional heat generated in the early stages of an orbital friction welding process," *Wear*, vol. 114, no. 3, pp. 355–365, Feb. 1987.

Vita

Karan Shirish Antrolia was born in Kolkata, state of West Bengal and the country of India on December, 1st 1993. He was raised in Mumbai, India. He graduated with Bachelor of Engineering in Production Engineering from University of Mumbai in May 2015. Enrolled at Lehigh University in January 2016 to pursue a Master of Science in Mechanical Engineering. During his period at Lehigh University, he has served as research assistant for four semesters and worked on various research projects under the guidance of Prof. Herman Nied. These research projects were a collaboration of Lehigh University with SAFRAN and Fraunhofer IWM. During his graduate work, Karan earned a Young Scientist grant from the German government.